CHALMERS

Evaluation of scintillation materials and silicon photomultiplier for dosimetry

Master of Science Thesis in the Master Degree Programme Biomedical Engineering

MATTIAS JÖNSSON

Department of Signals and System
Division of biomedical engineering
CHALMERS UNIVERSITY OF TECHNOLOGY
Performed at Unfors Instruments AB
Göteborg, Sweden, 2010
Master's Thesis 2010:091

Evaluation of scintillation materials and silicon photomultiplier for dosimetry

MATTIAS JÖNSSON

Department of Signals and System

CHALMERS UNIVERSITY OF TECHNOLOGY

Göteborg, Sweden 2010

Evaluation of scintillation materials and silicon photomultiplier for dosimetry

MATTIAS JÖNSSON

Department of Signals and System
Chalmers University of Technology
SE-412 96 Göteborg
Sweden
Telephone + 46 (0)31-772 1000

[Chalmers Reproservice]
Göteborg, Sweden 2010

Evaluation of scintillation materials and silicon photomultiplier for dosimetry

MATTIAS JÖNSSON
Department of Signals and System
Chalmers University of Technology

Abstract

Scintillators have been widely used in radiation detection for almost one century. It has traditionally been used together with a photomultiplier tube (PMT) but in recent years silicon photomultipliers (SPM) has begun to compete with the PMT. This opens opportunities for new applications like pocket size dosimeters. The purpose of this thesis is to investigate the use of different scintillator materials combined with a SPM to make dosimetry on a wide energy spectrum and to do sensitive detection of low dose rate.
Four different scintillators were investigated whereof one plastic and the others inorganic, the scintillators were BC-428, BGO, LYSO(Ce) and CsI(TI). The SPMs used were from Sensl and contained two different variations, both with the area of 2.85x2.85 mm but with 20x20 µm respectively 35x35 µm microcell size, called SPM 3020 and SPM 3035.

The best combinations for dosimetry in the diagnostic energy range is CsI(TI) with SPM 3035 and SPM 3020, resulting in a dose rate approximation within 6 percent (compared to the PTB calibrated Xi survey probe used for reference) for energies between 32- and 96 keV. Clear spectrums for energies down to 17 keV were obtained with the SPM 3035 combination. The other detection solutions are not applicable for the used energies.

The capability to detect low dose rates was found to be exceptional since background radiation (0.1µGy/h) could be measured with one count per second (CPS).

Keywords: scintillator, silicon photomultiplier, SPM, dosimetry

Acknowledgments

First and foremost I would like to thank Per Klockar for the opportunity to perform this thesis and for great support and help during the course of the work. Fredrik Oskarson and Raine Vesanen have also been of great assistance. I would like to thank Anders Lindstöm for help with Lab View and Johanna Torell for giving up her desk for me. Jakob and Jakob also deserve special thanks for great social support. At last thanks to everybody else at Unfors who made my time here a pleasant experience.

Abbreviations

SPM	Silicon PhotoMultiplier
PMT	PhotoMultiplier Tube
PDE	Photon Detection Efficiency
PDP	Photon Detection Probability
CPS	Counts Per Second
APD	Avalanche Photo Diode

Table of Contents

1 Introduction

1.1 Background

Scintillation is an established technique which is widely used in all kind of radiation detection. The basic physics is that radiation energy is absorbed in the scintillator and then reemitted as light photons. These photons are then measured to determine the initial radiation dose. Scintillation was introduced in the beginning of the 20th century but gained popularity when the photomultiplier tube (PMT) was introduced and improved as a scintillation counter in the 1940 and 50s [12]. The PMT has been the main choice for photon detection ever since due to the fact that they have high quantum efficiency and high amplification [12]. Lately however semiconductors have begun to compete with the PMT, the photo diode for example which has higher quantum efficiency in the visible range and above, lower power consumption, smaller size, more rugged etc. The drawback is that the conventional photodiode does not have any internal gain which leads to a smaller output signal which consequently makes it more sensitive to low level noise [1].

To improve the gain an avalanche photodiode (APD) can be used, it has a gain in the range of hundreds combined with most of the benefits of the conventional photodiode. The gain is due to a high electrical field which accelerates the electron. The acceleration gives the electron enough energy to ionize another electron-hole pair when it collides with the crystal lattice. Both these electrons can then accelerate again creating more electron-hole pairs.

The gain in the APD is however very sensitive to changes in temperature and applied voltage [1]. To get an even higher gain and decreased sensitivity to temperature the APD can be used in Geiger mode. Geiger mode is when the APD is reversed biased above the breakdown voltage, this gives a gain in the range of the PMT (10^6) and makes it possible to use in room temperature [5] [7].

When used in Geiger mode the APD will be either on or off and the output of the APD will be the same regardless of the number of light photons that triggered it. In other words the

intensity of the incident light photons is lost in a single APD. To address this problem an array of APD are used [7]. They go under the name multi-pixel photon counter (MCCP) or silicon photomultiplier (SiPM or SPM). Such a device can be seen as the as the solid state analogous to the PMT.

Dosimetry is the measuring of absorbed radiation dose. There are two kinds of dosimerters, passive and active. Commonly used passive dosimeters are the Thermo Luminescent Dosimeter (TLD) and the film badge. To get a real time value of your exposure you can instead use an active dosimeter, typically an electronic personal dosimeter (EPD). The passive and the active dosimeters are often used together to complement each other. The room for improvement lays mainly at the EPS and some things that are desirably to improve are the detection of low energies and low dose rates. For real time measurements the response time is also of importance.

With new image analysis/processing techniques and better hardware the radiation dose needed to get a good X- ray image is decreasing. This increase the need for more sensitive detection devices. Overall increased awareness of the biological effects of radiation also contributes to a higher demand for a versatile product.

1.2 Aim of study

The purpose of this thesis is to evaluate and investigate the possibilities to use scintillator materials in combination with the silicon photomultiplier to be able to do dosimetry on a wide energy spectrum and to do sensitive detection of low dose rates.

1.3 Delimitations

Energy absorption in matter is a complex field and differs depending of the characteristics of the incident radiation. This thesis will only deal with the interaction of electromagnetic radiations hence discarding electrons, neutrons and heavy charged particles.

Self absorption of the light emission will be neglected due to small size detectors. It is also of importance that the solution is commercially available in order to make a difference, hence components have to be reasonably priced.

The unlinearity in the light yield from the scintillators at different energies will not be compensated for.

1.4 Methods

To investigate the properties of different scintillator material combined with SPMs to detect low dose rates and to do dosimetry on a wide energy spectrum a measuring set up was constructed. Measurements were conducted in a X-ray laboratory at varying energies and dose rates. The data were analyzed and compared to reference measurements.

2 Theoretical background

2.1 Energy absorption in matter

There are three primary interactions for energy absorption when a scintillator is hit by photons. Each one will be briefly described in this section.

2.1.1 Compton scattering

When a photon hits a free electron (the photon energy >> electron binding energy) in the absorbing material and is deflected with an angle θ it is called Compton scattering. Energy is transferred from the incident photon to the electron and the amount of energy in the recoil electron relates to the original photon energy according to equation (1), where $\alpha = E/m_0c^2$, m_0c^2 is the rest mass energy of the electron = 0.51 MeV, $E = hv$, h = Planck's constant and v = frequency. The possibility for a photon to scatter is related to the electron density and increases linearly with the atomic number.

$$T_c = \frac{\propto E(1-cos\theta)}{1+\alpha(1-cos\theta)} \quad (1)$$

The scattered photons energy is given by equation (2)

$$E' = \frac{E}{1+\alpha(1-cos\,\theta)} \quad (2)$$

In the extreme case of $\theta = \pi$ the photon energy and the electron energy is given by equation (3) and (4)

$$E' = \frac{E}{1+2\alpha} \quad (3)$$

$$T_{cm} = \frac{E}{1+(1/2\alpha)} \quad (4)$$

If the angle is larger than 120 degrees the energy of the scatted photons will be almost identical, this process is referred to as backscattering. Backscattering gives rise to a peak at 0.256 MeV or less, called a backscatter peak. This is because for large energy photons equation (3) can be written as equation (5), showing that this is the maximum achievable energy.

$$E' = \frac{m_0 c^2}{2} = 0.256\ MeV \qquad (5)$$

Since Compton scattering occurs at all angels it will have a continues spectrum up to the Compton edge at $\theta = \pi$, which according to equation (5) is located at $E - 0{,}256\ Mev$ [4] [1].

2.1.2 Photoelectric effect

For all the energy in the incident photon to be absorbed the electron has to be bound in the atom. When the electron is hit it is ejected from the atom and is then called a photoelectron. The energy of the photoelectron is given by equation (6).

$$T_p = E - B_e \qquad (6)$$

Where E is the energy of the incident photon and B_e is the binding energy. It is most likely that electron is ejected from the inner layer of the atom typically the K or L shells. When the vacancy from the photoelectron is filled characteristic X-rays or Auger electrons is created. The Auger electron is always reabsorbed but the characteristic X-ray can escape without further interaction in the absorber material. The likelihood for the photoelectric effect to happen depends on the photon energy and the atomic number according to equation (7). Where n depends on the photon energy and varies between 4 and 5. At high energies typical in the range of a few MeV the photoelectric effect no longer has any impact.

$$\tau \cong constant * \frac{Z^n}{E_\gamma^{3.5}} \qquad (7)$$

Since most often all the energy of the incident photon is absorbed in the photoelectric effect, this is the preferred way of absorption to get maximum energy exchange. Hence high atomic

number is important when choosing a detector for X-rays. The photoelectric effect gives rise to a photopeak which contains the full energy of the incident photons, unless energy has been lost due to escaping characteristic X-rays [1] [4].

2.1.3 Pair production

If the incident photons energy exceeds $2m_oc^2$ (the mass of the electron + the positron) pair production becomes possible. The photon is then completely absorbed and an electron-positron pair is created, its kinetic energy is given by equation (8)

$$T_{pp} = E - 2m_oc^2 \qquad (8)$$

The positron and the electron will slow down in the absorbing medium and deposit all its kinetic energy. The positron will then interact with an electron resulting in two annihilation photons at energies of 511 keV. These can either be absorbed by Compton scattering or the photoelectric effects, or one or both can escape. The resulting energy if both photons escape is called the "double escape peak" and is consequently located at $hv - 2m_0c^2$. If only one photon escapes the "single escape peak" is located at $hv - m_0c^2$.

The probability of pair production increases with high energies and do not give any effect before the energy is several MeV, after this the pair production impact rises sharply. The dependence of the absorber material can be approximated as the square of the atomic number [1] [4].

2.2 Pulse shaping

Pulses from radiation detectors are often shaped in an undesirable way i.e. sharp slopes and fast peaks. A preamplifier often produces a train of pulses and if the tail of one pulse not has time to fully decay the next one will gain amplitude. This will give rise to peaks that looks higher

than they really are which is clearly undesirable. Even if the pulses are fully separated the shape can make them difficult to detect for example a sharp fast peak could need really fast sampling to get a good peak value. To address these problem pulse shaping is used. One way to accomplish this is to use a CR-RC network. The CR part is called a differentiator since it produces an output that is proportional to the time derivative of the input. The RC part works as an integrator and produces an output that is the integral of the input. For this to work the time constant $\tau = RC$ has to be sufficiently small compared to the duration of the input pulse. If multiple RC stages are used after the CR stage the resulting signal will have a Gaussian shape [4].

2.3 The scintillation process in inorganics

The scintillation mechanism in an inorganic crystal depends on the energy states of the crystal lattice. The valence band and the conduction band are separated by a forbidden band where no electrons can be found. A perfect crystal lattice will have a large band gap and the amount of charge carriers will be negligible at normal temperatures. If however an electron is elevated to the conduction band the de-excitation will be an inefficient process and the wavelength will be too small to be in the range of visible light.

To redress this and get a good light yield an impurity is added, called activator. The activator creates sites in the forbidden gap where de-excitation can occur. This makes the band gap smaller and the emitted photons will be in the visible range. As a charged particle pass through the crystal electrons will be elevated from the valence band to the conduction band. This creates electron hole pairs and the holes will find an activator site to ionize. When an electron finds an activator site, it might recombine and de-excite to the ground state. This requires that the transition is allowed and will then result in photon emission which is very likely to be in the visible range.

If the transition to ground state is forbidden more energy is needed before de-excitation, for example thermal energy. This process is referred to as phosphorescence and has a longer time

constant. The phosphorescence gives rise to what is called “afterglow” or the “slow component” in some scintillators. In pulse mode this afterglow will result in pulses with lower amplitude which can be resolved easily. In current mode or at high counting rates the result will however be an amplitude offset which is an undesirable effect [1].

In the conversion to scintillator light there also exists some lose mechanisms called quenching, this is when the excitation energy is dissipated by radiationless thermal transitions. The quenching processes give rise to the nonlinearity that can be observed in inorganic scintillators, the nonlinearity is however much less than in the organics.

Since the energy needed to create the initial electron hole pairs is larger than the impurity emission the crystal lattice is transparent to this which makes self absorption negligible. For pure crystal scintillators this effect is significant and limits their use to small sizes.

2.4 Scintillation process in organics

In an organic molecule the light emission emerges from the transitions between different energy levels. When a charged particle passing by its kinetic energy is absorbed by the molecule causing it to excite to a higher energy state. The small steps in figure (1) represent vibrational steps. Compared to thermal energy in room temperature these steps are large. This results in that most molecules in room temperature are in S_{00} state. A molecule excited to higher states than S_1 are rapidly deexcited to the S_1 state due to radiationless internal conversion. If the molecule is excited to the vibrational steps surrounding a higher state it is also quickly returned to the main step since the vibrational steps not are at thermal equilibrium. This results in that the fluorescent light from an organic scintillator comes from the transitions from S_{10} state. This process is fast compared to the inorganics with typical decay times in the size of a couple of nanoseconds.

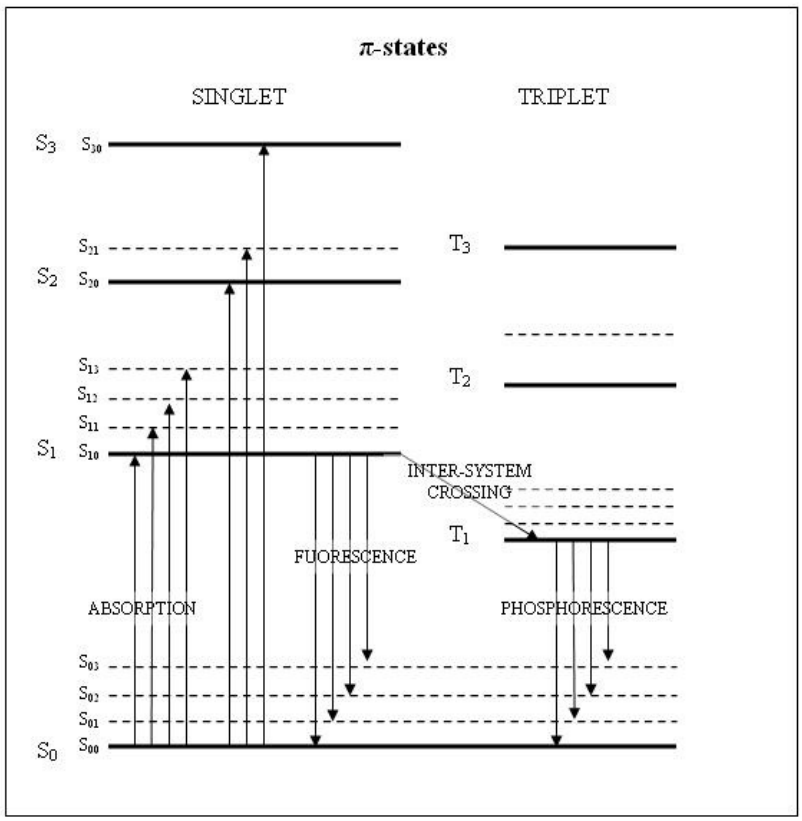

Figure 1 The π-states of an organic molecule

Some molecules can cross over to the triplet states, the decay time here is much higher than for the singlet states and the wavelength is longer since the energy gap is smaller. The deexcitation from these states gives rise to phosphorescence.

Once in the T1 state thermal energy can excite the molecules back to the S1 state, where the deexcitation then occurs. This is called delayed fluorescece. Since almost all the fluorescence is emitted at a shorter wavelength than the absorption the self absorption is small.

2.5 Scintillation materials

The materials dealt with in this thesis will be disused in this section. It will mostly be inorganics since they are better at detecting gamma and X-rays. This is due to their high density and

atomic number which gives a high electron density. The more electrons there are for the incident photons to collide with the higher the probability that this occurs [1]. One plastic scintillator will also be included since the density of plastics is very close to 1000kg/m^3 which give a good body equivalent response since the human body contains 70% water. The inorganic will however yield less light and suffer from lower detection probability. The linearity for low photon energy will also be a problem [11]. The decay time for the plastic scintillator is very good compared to the inorganics which will be an advantage in high dose rate measurements. The coupling to the detector consists of an epoxy layer with refractive index of about 1.53 [14] which mean that you get the most effective light collection when the refractive index of the scintillator matches this.

2.5.1 NaI(TI)

Sodium iodide is the most widely used scintillator in medical applications. For the purpose of dosimetry however it is not so suitable for a commercially available dosimeter because it is hygroscopic. The hygroscopicity results in a need for a hermetic capsulation. One other drawback is that it is not as rugged as some other materials and can be damaged by thermal or mechanical shock. It is often referred to and compared with in the litterateur and that is why it is mentioned in the thesis. NaI(TI) emission spectrum peaks at 415 nm and the light yield is 38000 photons/MeV. Because of the phosphorescence disused in 2.3, sodium iodide also have some problem with afterglow which is a problem at high counting rates [1]

2.5.2 LYSO(Ce)

Cerium doped lutenium yttrium oxyorthosilicate is a newly developed crystal with great characteristics. It is non hygroscopic, has fast decay time (40ns) and high stopping power. The fast decay time makes it suited to detect high counts of X-ray. The emission wavelength is

420nm, the effective atomic number is 66, the density is 7,1 g/cm3 [3] and the refraction index 1.82 [2]. LYSO(Ce) has a light yield of 27000 photons/MeV [13].

2.5.3 CsI(TI)

Cesium iodide with thallium activator has an effective atomic number of 54 and a density of 4.51 [3]. CsI(TI) is somewhat hygroscopic and should not be subjected to high humidity or water. CsI(TI) is more rugged than NaI(TI) and can therefore be used in applications which need higher tolerance against vibration etc. CsI(TI) has different decay times for different particles (680ns and 3340ns) and can be used to determine between different kinds of radiation[1].

The emission spectrum is peaked at 540-560 nm [3][2] which could be a problem since most photo detectors is optimized for lower wavelengths, but with a detector in the right range the light yield is the highest of all scintillators with 65000 photons /MeV [1]. CsI(TI) has a refraction index of 1.78 [2]. CsI(TI) has a nonproportionality of the light yield for energies below 100 keV. To use CsI(TI) as a detector for low photon energies consideration has to be taken to this when calibrate the instrument [15].

2.5.4 BGO

Bismuth Germanate has a high effective atomic number of 74 and a high density of 7.13 g/cm3 [3] which gives it the highest probability of all common scintillators for the photoelectric effect to happen. The peak emission spectrum is located at 480nm and the light yield is quite low at 8200 photons/MeV [13][1] . BGO is more rugged than NaI(TI) and is non hygroscopic which makes it well suited for small handheld or pager like dosimeters [1]. BGO has a quite high refraction index of 2.15 which makes light collection more difficult compared to scintillators with lower values. The self absorption is low due to the differences in the emission spectra and the optical absorption.

2.5.5 BC-428

A plastic scintillator with peak emission at 480nm which match the Sensl SPMs peak spectral response very well [10].Measured characteristics from [11] shows a little aberration compared to the manufactures specifications, for example the measured light yield is twice as high as the reported one of 36% of Anthracene. The density of BC-428 is 1032 kg/m^3 which as mentioned above is close to water and therefore gives a good tissue equivalent response. The refraction index is 1.58 [10] which are very close to the epoxy refraction index between the scintillator and the detector. The base material is polyvinyltoluene [10] which has the chemical formula $C_{27}H_{30}$ [21]. This gives an approximated effective atomic number of 5.66.

2.6 Scintillation detectors

Some common type of detectors for scintillation is photomultiplier tubes (PMT), photodiodes (PD) and the silicon photomultiplier (SPM).

2.6.1 Photomultipler tube

Photomultipler tubes (PMT) are a photon detection device that uses the photoelectric effect combined with secondary emission [12]. It consists of a vacuum tube in order to efficiently accelerate the low energy photons through the tube [1]. As shown in figure (2) it has an input window and on the inside of the window a photocathode is placed. The photocathode consists of an alkali metal with a very low work function, for example cesium and antimony, which means what the energy needed for the photo electric effect to happen is low [12]. The electrons that is ejected from the photocathode then passes trough a focusing electrode before it hits the first dynode (electron multiplier). At the dynode the electrons are multiplied by secondary emission [12]. The next dynode has a higher voltage which makes the electrons released from the first to accelerate towards it. At each dynode 3-4 electrons are released for

every incident electron, and with 10 to 14 dynodes the gain will be in the range of 10^6 to 10^8 when they reach the anode [18]. Typical operating voltages are in the range of 500 to 3000 V [12]. The PMT is sensible to electromagnetic fields. The quantum efficiency is defined as equation (7).

$$QE = \frac{number\ of\ photoelectrons\ emitted}{number\ of\ incident\ photons} \quad (7)$$

In the PMT the quantum efficiency is limited to 20-30 %. The absorption in the photocathode depends on the wavelength of the photons. This leads to that the emission spectrum of the scintillator strongly affects the quantum efficiency, hence it is important to match these against each other to get the best performance [1].

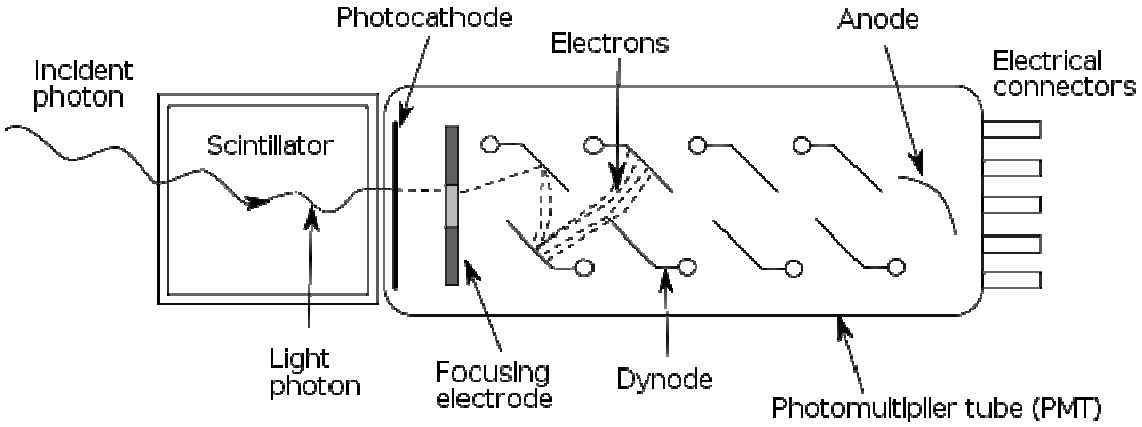

Figure 2 Schematic of a PMT

2.6.2 Photodiodes

Another way of detecting photons is by using a photodiode, a conventional photodiode most often refers to a PIN diode. PIN means that the p and the n doped sides are separated by a depleted i-region. When the diode converts photons to into electrical signals the energy of the

incident photons must exceed the bandgap of the detector, typically 1-2 eV. The photons are then absorbed and an electron is excited from the valence band to the conduction band leaving a hole behind. The doping gives rise to an electric filed which makes electron drift to the n-side and the hole to the p-side. This results in a photocurrent that is the output of the diode [1][7]. The charge is however not amplified making the output signal amplitude small. This makes the photodiode sensitive to electronic noise. The quantum efficiency for the photodiode is high (60-80%) compared to the PMT (20-30%) which gives a higher energy resolution. The wavelength span is also wider typically 500-900nm in silicon.

2.6.3 Silicon PhotoMultiplier

The Silicon PhotoMultiplier (SPM) was developed in Russia in the mid 1980s and it uses an array of avalanche photodiodes (APDs) to get a good sensitivity for small numbers of photons [17]. In the avalanche photo diodes the same thing happens as in the ordinary photodiode but in the APD there is a high electrical field which accelerates the electron when it enters this region. The acceleration gives the electron enough energy to ionize another electron-hole pair when it collides with the crystal lattice. Both these electrons can then accelerate again creating more electron-hole pairs. This gives an internal gain to the diode typically in the size of hundreds [6].

The impact ionization gives rise to an error called multiplication error which origins from the fact that the actual number of electron-hole pairs generated per incident photon varies between the events. If the gain is increased the multiplication error gets worse [7].

The APDs are operated in Geiger-mode to increase the gain. In Geiger mode the diode is reversed biased higher than the breakdown voltage. Reversed biased means that the negative pole of the battery is connected to the P-doped region and the positive pole to the N-doped region. The depletion zone is then widened and the diode will not conduct any current until it breaks down. [8]

The Geiger-mode operated APD is stable above the breakdown voltage but when an electron enters the region of high electric field the junction breaks down and diode becomes a conductor. This process is called a Geiger discharge. The relationship between applied voltage and gain is linear and the gain is in the range of 10^5 to 10^6, which is comparable to the PMT. In order to detect multiple photons you need to couple the APD in parallel, since in the single diode it is impossible to say if the Geiger discharge was triggered by one or multiple photons. If connected in an array the output will be the sum of all APD and it will then be possible to determine if the input was a single or multiple photons. An APD operated in Geiger mode will not suffer from multiplication noise like an ordinary APD since the probability of impact ionization does not affect the output. If the avalanche process does not die out the output will be the same for all events [7]. The Geiger mode operated APD is instead concerned with the photon detection probability (PDP) which is the quantum efficiency multiplied with the avalanche probability [7]. To get the photon detection efficiency (PDE) you scale the PDP with a fill factor, the PDE of a SPM depends on the wavelength and the bias voltage and is given by equation (9).

$$PDE(V,\lambda) = \eta(\lambda) * \varepsilon(V) * F \tag{9}$$

Where $\eta(\lambda)$ is the quantum efficiency in silicon, $\varepsilon(V)$ is the avalanche probability and F is the fill factor. The fill factor is the ratio between the active area of the SPM and the total area [17]. The more pixels you have on a fixed area the worse the fill factor will be, it will also depend on the shape of the active silicon area. The dynamic range of the SPM is given by the PDE and the total number of microcells. The number of fired microcells is given by equation (10).

$$N_{fired} = N_{total} * \left[1 - \exp\left(\frac{-N_{photon} * PDE}{N_{total}}\right)\right] \tag{10}$$

Where N_{fired} is the number of excited pixels, N_{total} is the total number of pixels and N_{photon} is the number of incident photons [16].

The SPM stays linear when approximately less than 25% of the pixels have fired. To make the SPM able to coop with higher photon fluxes (extend the linearity), you can decrease the PDE. This is done by reducing the operating bias since the avalanche probability depends on that according to equation (9) [17].

If an electron-hole pair is thermally generated it is called dark current since this could happen without any incident photons. The dark current leads to detection errors called dark count, this problem can be redressed with lowering the temperature. In room temperature the dark rate is in the range of MCPS (count per second) and in -20 degrees it range of tens of KCPS, there is also an influence of the fill factor which states that a lower fill factor reduces the dark rate.

Another reason for dark current can be poor quality material and insufficient fabrication techniques [5] [6] [7].

If the dark rate can be measured it can then be subtracted from the signal hence reducing the influence. Some statistical variations is however impossible to compensate and sets the minimum detectable signal [17].

When the Geiger discharge is released photons can be generated that trigger other APDs leading to an unwanted effect called crosstalk. Crosstalk causes the output from the SPM to be higher than the energy detected. The amount of crosstalk is proportional to the overbias and by lowering it you can reduce the effect [22]. Higher fill factor also has a negative influence on the crosstalk. Another way to reduce the crosstalk is to optically isolate the pixels [17].

Afterpulses are also a problem with the SPMs, this occurs when charge carriers are trapped in a bandgap state. When the carriers are released at some latter point they can cause new avalanches. The probability for a carrier to be trapped increases with lower temperature[5].

The operating voltage also influence the afterpulses and an increase in the over bias increases the probability for an afterpulse [17]. A hold off time can also be used to minimize the influence of afterpulses since most of the afterpulses occur within a few hundred nanoseconds after an avalanche pulse, this however acquire an active quenching circuit [20].

Afterpulses and crosstalk are both problems that dope the PDE value of the SPM and needs to be taken into account to get an accurate measurement of the incident photons.

Some advantages of the SPM is that it is insensitive to magnetic fields, small, rugged, inexpensive and it often has a higher photon detection efficiency than the PMT (due to higher quantum efficiency) [5].

Once the APD has triggered it needs to be reset so it can detected the next photon. This can be accomplished in two ways either by an active or a passive quenching circuit [7]. In passive quenching a resistance is placed in series to the diode. When the Geiger discharge is released large current flows through the resistor causing the voltage to drop in the APD, which then can be recharged [5]. The quenching time for a passive circuit is in the order of microseconds.

To get a faster quenching time an active circuit can be used instead, it uses switches to recharge and to quench the APD, this gives quenching times as low as 1.5 ns [9].

If the temperature rises other processes will interfere with the impact ionization, this will cause the current released in the Geiger discharge to decrease hence lowering the gain and make the APD more sensitive to noise [7]. On a 1600 pixel (25 μm) SPM from Hamamatsu the gain decreases with 1,1% per degree [19]. Still the SPM will operate well in room temperature but some temperature monitoring could be needed [6].

Some typical applications for the SPM are PET, SPECT, PET/MRI and radiation detection i.e. scintillator readout.

3 Methods

3.1 Experimental setup

For the experimental setup a “dark box” was needed because of the high sensitive of light photons of the SPM detector. This was constructed using an aluminum box and some panel contacts, one for the power supply and one for the signal output. A hole in the top of the box was made to allow radiation to enter the scintillator. The hole was covered by aluminum tape to filter out the light. The “dark box” is displayed in figure (3).

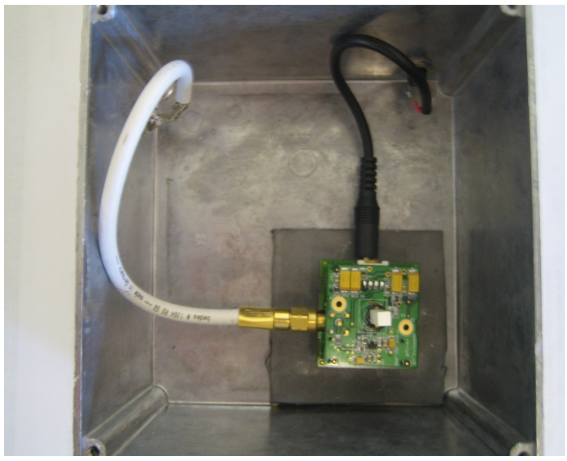

Figure 3 "dark box"

Inside the “dark box” the SPMA4 power and preamplifier board was installed. Below the circuit board a lead plate was placed to reduce the influence of scattered radiation. Different combinations of the SPMs and scintillators were used. The equipment supplied in the SensL SPM Scintillator pack was three different SPMs:

- SPMMicro3035X13
- SPMMicro3035X13
- SPMMicro6035X13

And three different crystals:

- BGO
- LYSO(Ce)
- CsI(TI)

The plastic scintillator BC-428 were ordered separately from Bicron and painted with BC-620 reflector paint containing titanium dioxide to maximize the reflectivity. All the SPMs have a peak spectral response at 490 nm. When coupling the crystals to the SPM optic coupling grease (BC-630 silicon grease) was used to get maximum efficiency in the light collection. Because of the low sampling rate of the DAQ card a capacitance (10nF) was connected between the signal output and ground. The effect is a signal smoothing that enables sampling at the peak. This however slows down the pulse train and pile up problems appears at frequencies above 10-15 kHz.

3.2 Data processing

The data is processed in Lab View and a print screen of the environment is shown in figure (4). The output is a vector of the peak histogram i.e. the spectrum of the incident photon energies. To simulate a possible solution for dosimetry a channel interval approach was applied where a reference spectrum was taken with corresponding dose rates. An optimal weighting factor was calculated for each interval and applied to the corresponding channels. This energy compensation vector was evaluated on some test vectors with known dose rates. Freemat were used to perform the calculations.

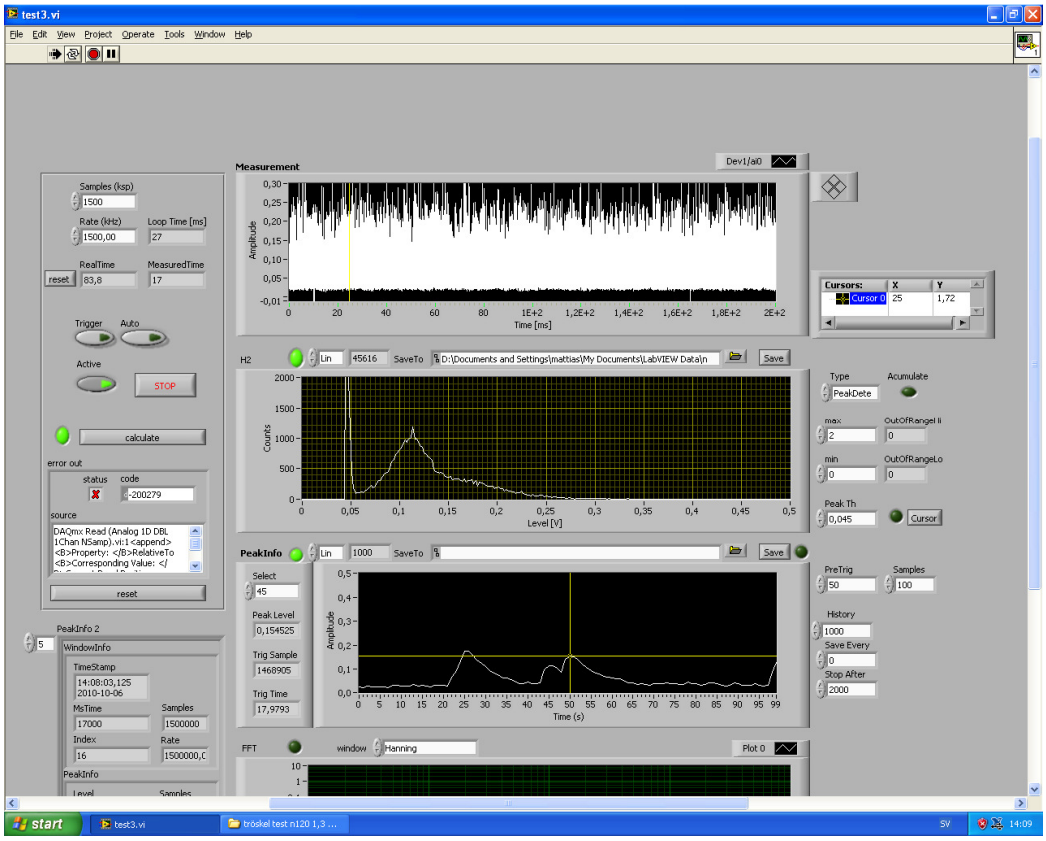

Figure 4 The lab view environment

The lab view environment (figure (4)) shows in the upper-most box the signal. In the second box the spectrum for one second is displayed and the third box gives information about the peaks. Tendencies of pulse pile up can be noted from both box 2 and 3, since the spectrums right slope not is as sharp as expected and the peak is a “double peak”.

4 Results

4.1 Saturation in the measuring set up

Because the limited sampling frequency of the data collection card the signal suffers from saturation when frequencies exceeds 10 KHz. This effect is shown in figure (5) where it clearly can be seen that with a higher threshold value the spectrum varies for a constant signal. In figures (6, 7) the saturation has not yet kicked in and this behavior is of course desirable. To get correct measurements this has to be taken into account and it limits the dose rate that is possible to measure.

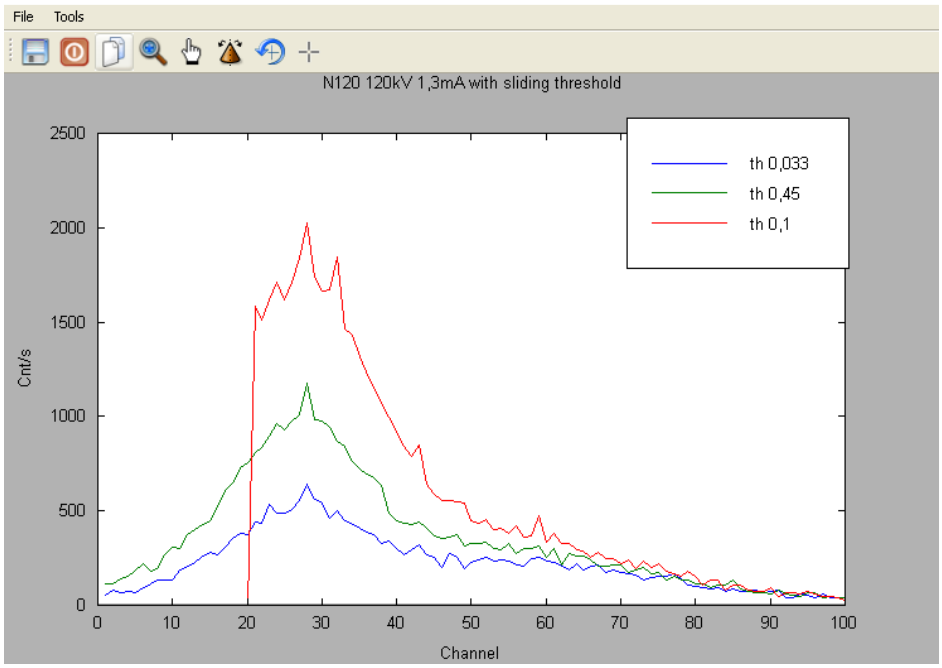

Figure 5 Example with saturation

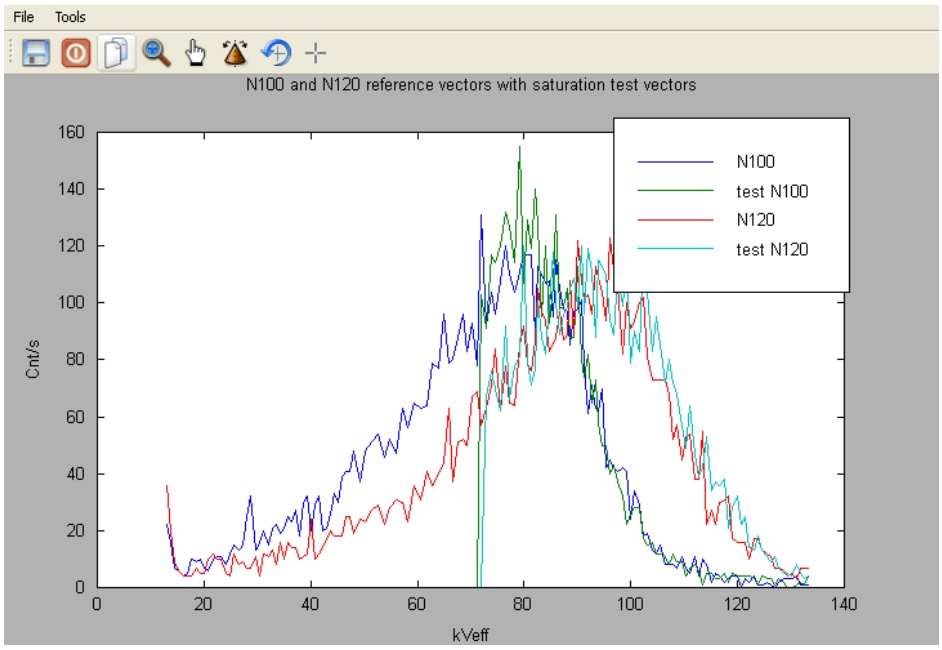

Figure 6 Example without saturation

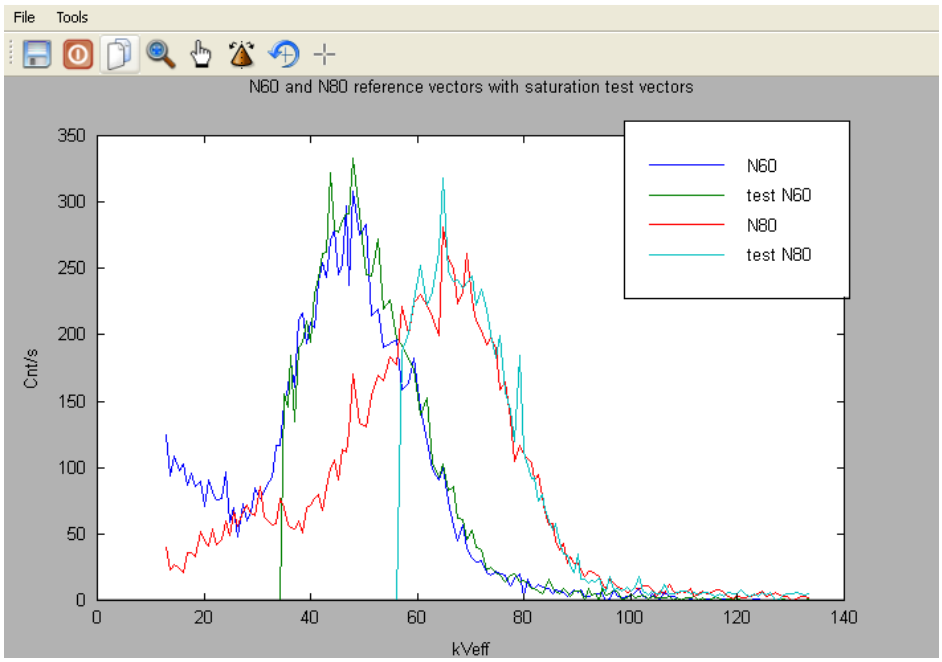

Figure 7 Example without saturation

4.2 Energy dependence

If a scintillator dosimeter only was to be used at one photon energy it could easily be calibrated to relate the count rate to dose rate. To measure dose rate at different incident photon energies however information about the photon energies and the detection efficiencies at that energies are needed. The photon response of the scintillator differs for different incident energies compared to air or tissue because of the difference in atomic composition. This is called energy dependence. Simplified energy dependencies for the different scintillators are displayed in figures (8-10). These are made under the assumption that the incident photon energies are monoenergetic i.e. all the counts from each radiation quality are assigned to one energy. The reference dose rate was measured using the Unfors Xi Survey probe. The dose rate is measured above the noise threshold since the noise fluctuates and adds uncertainty to the energy dependence. If the noise had been stable the measurements could be made with a lower threshold to then deduct the noise from the signal.

The energy dependencies below can be seen as the integrals of the spectrums display in figures (11-16).

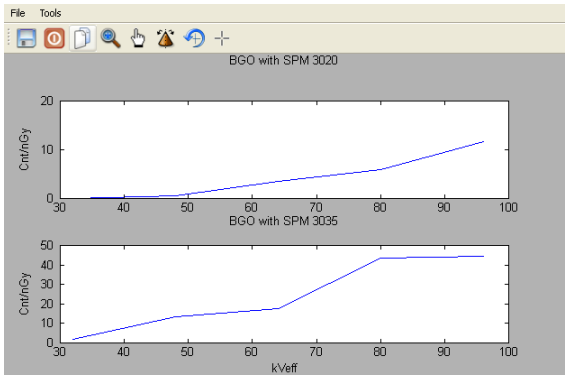

Figure 8 Energy dependence for BGO

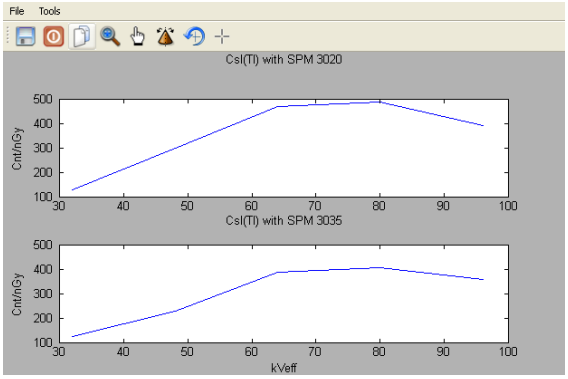

Figure 9 Energy dependence for CsI(Tl)

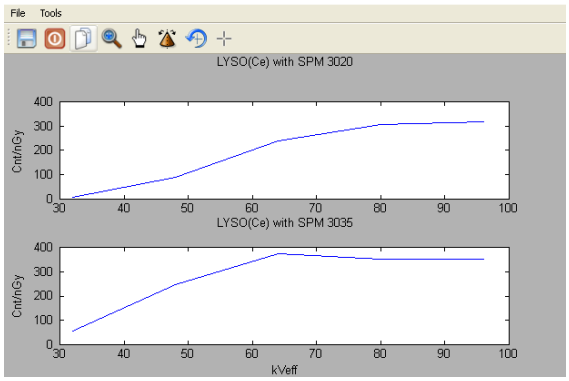

Figure 10 Energy dependence for LYSO(Ce)

In theory the inverse of the energy dependencies could be used to compensate for the energy dependence, but since the real signals not are monoenergetic and in fact the entire spectrum is available for analyze this will not yield a good result.

4.3 Spectrums for all scintillator SPM combinations

To obtain spectrums the N series filtration is used [Appendix A]. N series spectrums of CsI(TI) with SPM 3020 and SPM 3035 are displayed in figures (11,12). For the x-axis a kV_{eff} approximation is made which assumes that the channel with most counts for each signal quality is the kV_{eff} value, on the y-axis the counts are weighted with the dose rate. With the SPM 3020 52 channels are used and with the SPM 3035 150 channels. The flicker in the SPM 3035 case is due to the larger amount of used channels i.e. finer resolution. The overlaps in the spectrum are due to pulse widening in the system and the properties of the N series spectrum.

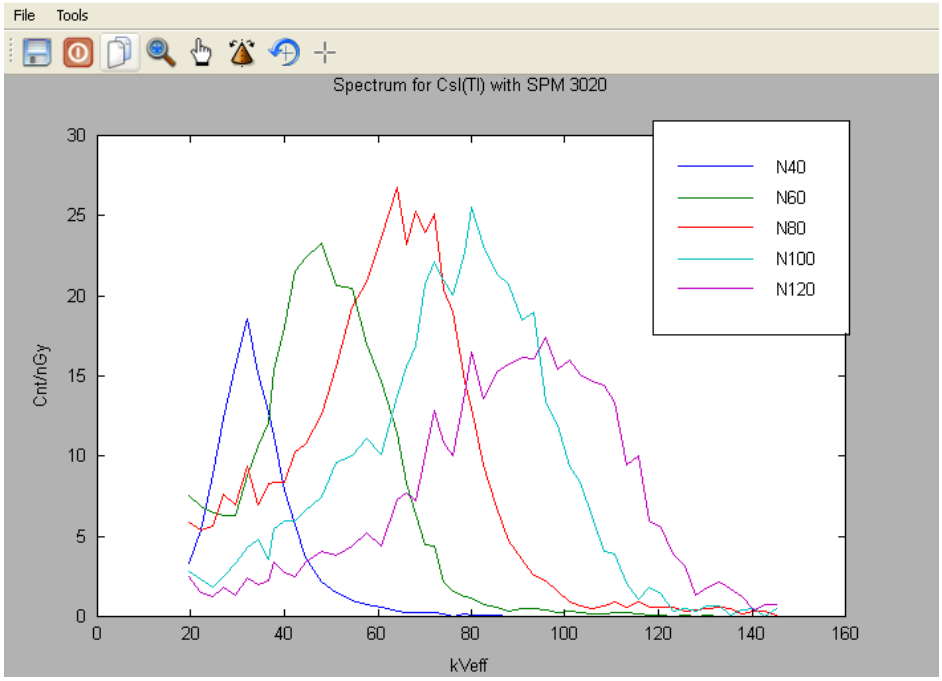

Figure 11 Spectrum for CsI(Tl) with SPM 3020

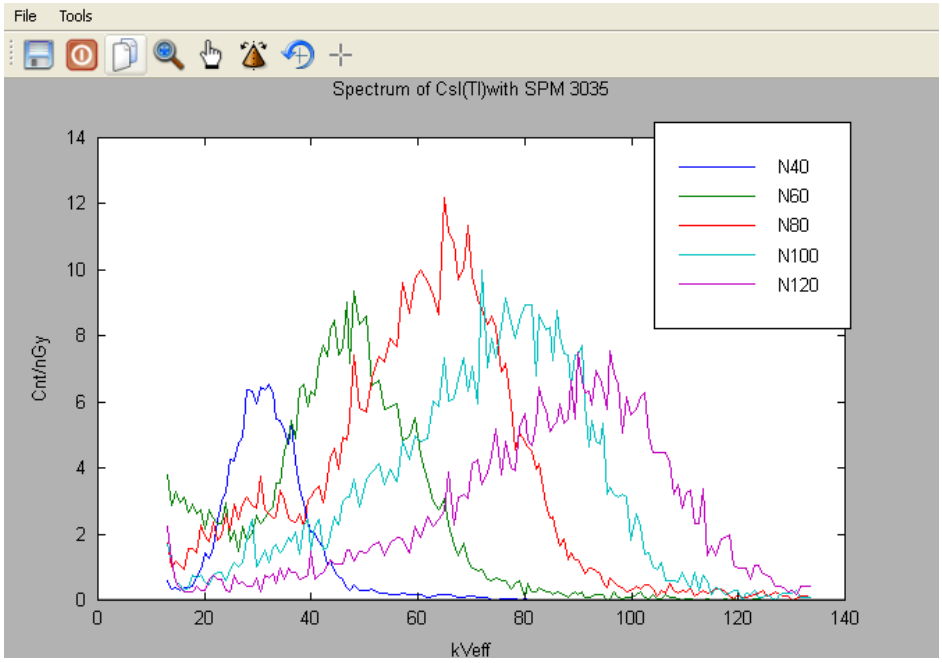

Figure 12 Spectrum for CsI(Tl) with SPM 3035

The N series spectrums for LYSO(Ce) are displayed in figures (13,14). With LYSO(Ce) 28 channels are used with SPM 3020 and 71 with SPM 3035. It can clearly be seen that the SPM 3035 resolves the spectrum much better than the SPM 3020 due to the higher PDE.

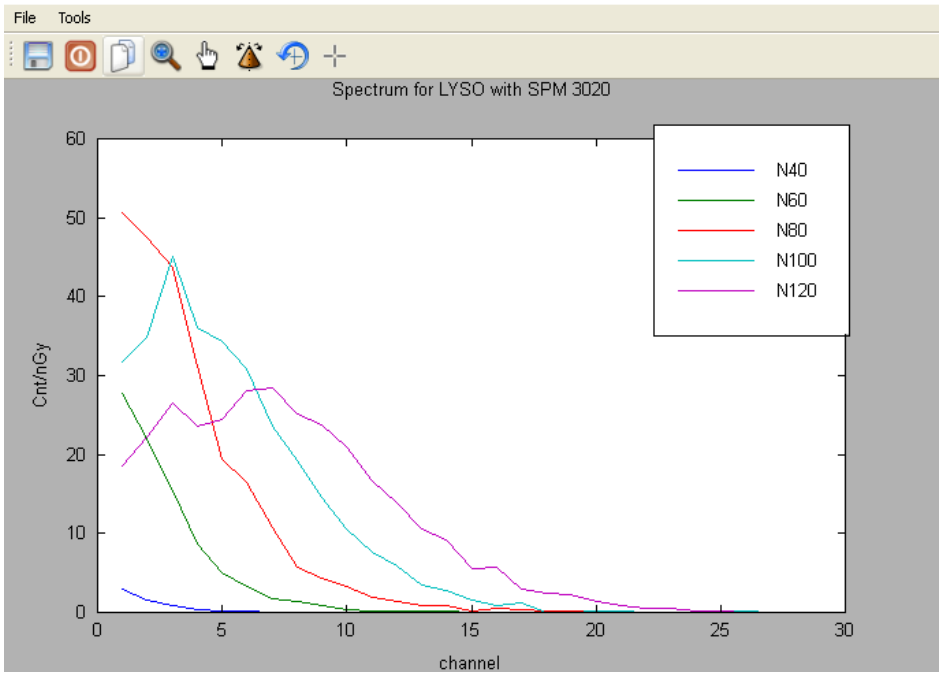

Figure 13 Spectrum for LYSO with SPM 3020

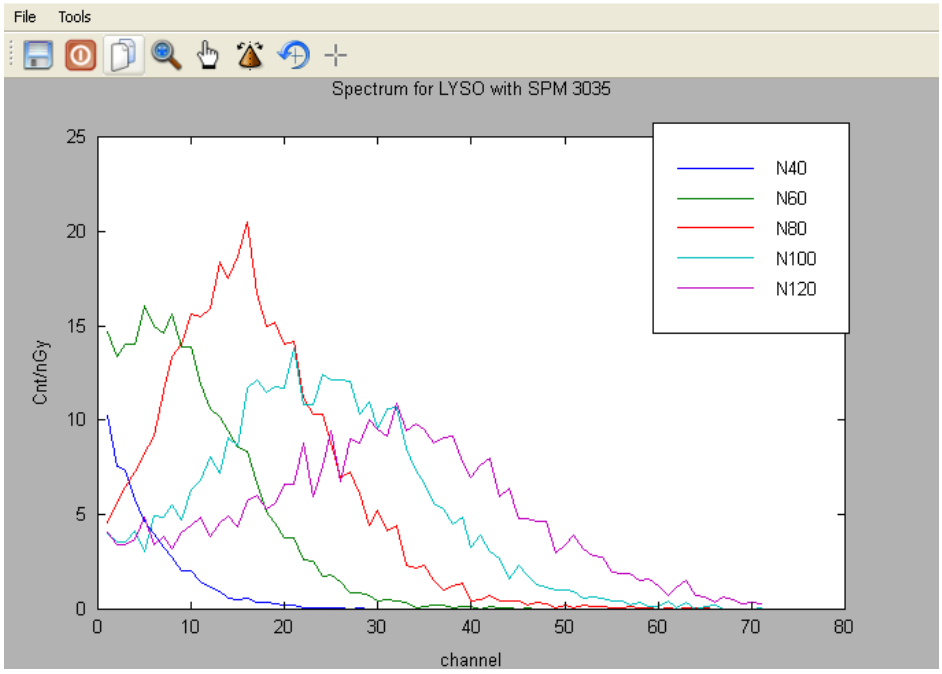

Figure 14 Spectrum for LYSO(Ce) with SPM 3035

N series spectrums of BGO are shown in figures (15-16). The lesser light yield from BGO becomes obvious and neither SPM 3020 nor SPM 3035 can resolve the spectrum from the noise. For SPM 3020 only 10 channels are used and for the SPM 3035 20 channels.

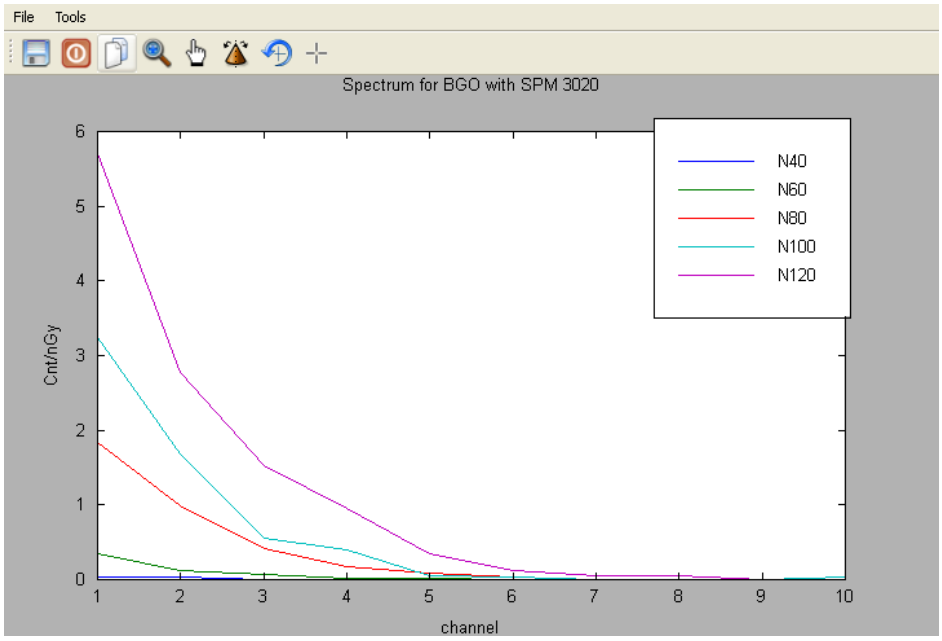

Figure 15 Spectrum for BGO with SPM 3020

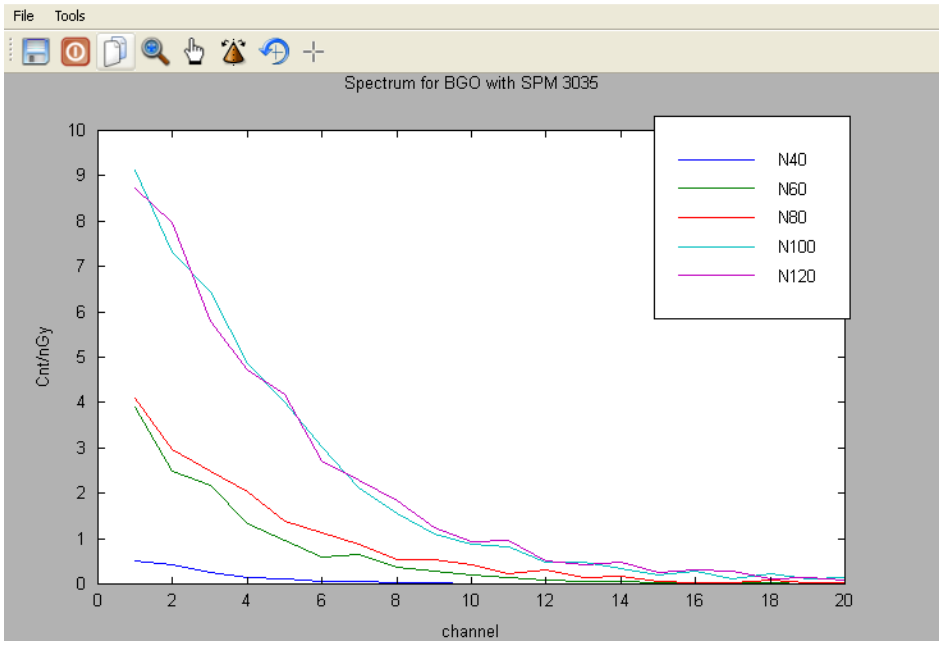

Figure 16 Spectrum for BGO with SPM 3035

4.4 Dosimetry

To use the spectrum information to make energy compensation i.e. compensate for the difference in the photon response for different energies, the spectrum is divided into five blocks. An example of the intervals for CsI(TI) with SPM 3020 is shown in figure (17).

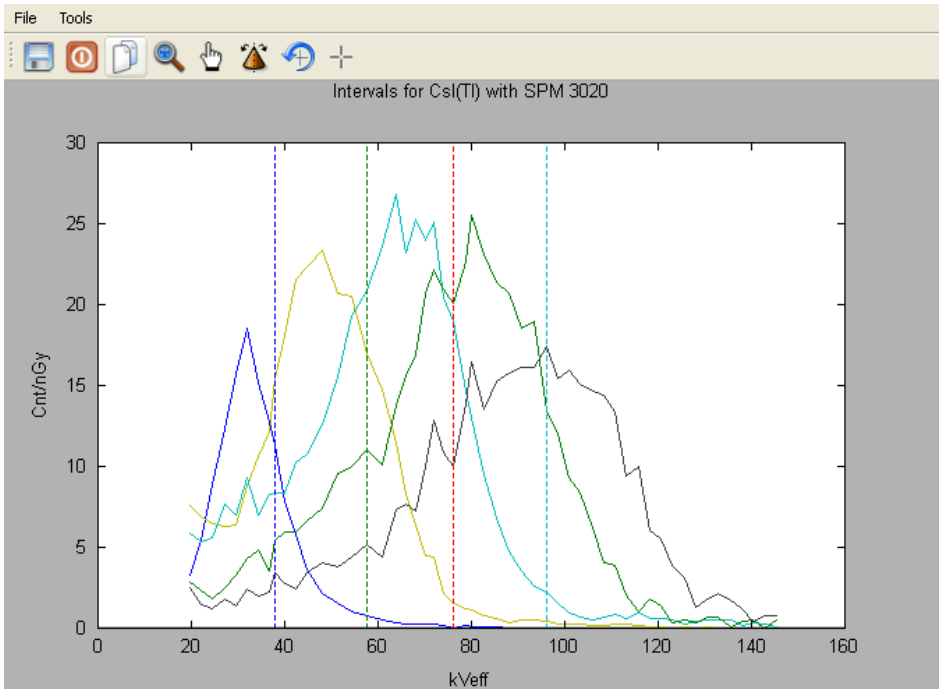

Figure 17 Energy compensation vector intervals for CsI(TI) with SPM 3020

Each vector is assigned a reference dose rate, measured with Unfors Xi Survey probe. It is desirable that each vector has most counts in the interval that represents that vectors radiation quality. An example for CsI(TI) with SPM 3020 is displayed in equation (11), where each column represents the number of counts in one interval.

$$\underset{\mathbf{A}}{\begin{bmatrix} 5921 & 1301 & 122 & 22 & 3 \\ 2146 & 3826 & 1425 & 146 & 58 \\ 1289 & 1956 & 3745 & 1141 & 236 \\ 358 & 656 & 1620 & 1898 & 628 \\ 271 & 382 & 1032 & 1828 & 2008 \end{bmatrix}} = \underset{\mathbf{ref}}{\begin{bmatrix} 57.33 \\ 26.67 \\ 20.00 \\ 11.56 \\ 14.67 \end{bmatrix}} \quad (11)$$

The equation system is solved using Freemat command **A\ref=W** resulting in an optimal weighting vector **W**. The weighting vectors for all the scintillator SPM combinations are displayed in table (1). The unit of the weighing vectors are nGy/Cnt, resulting in the dose rate/channel when used on a random vector with counts/sec.

*Table 1 Weighting vectors (**W**) for all the scintillator SPM combinations*

SPM 3020			SPM 3035		
CSI(TI)	LYSO(Ce)	BGO	CSI(TI)	LYSO(Ce)	BGO
$\begin{bmatrix} 9.35\text{E}-03 \\ 1.41\text{E}-03 \\ 4.68\text{E}-04 \\ 2.30\text{E}-03 \\ 3.44\text{E}-03 \end{bmatrix}$	$\begin{bmatrix} 0.4669 \\ -2.4376 \\ 7.4516 \\ -9.6059 \\ 1.941 \end{bmatrix}$	$\begin{bmatrix} 44.6568 \\ 2.7736 \\ -381.889 \\ 62.5685 \\ 747.7151 \end{bmatrix}$	$\begin{bmatrix} 9.52\text{E}-03 \\ 1.25\text{E}-03 \\ 8.58\text{E}-05 \\ 1.82\text{E}-03 \\ 3.01\text{E}-03 \end{bmatrix}$	$\begin{bmatrix} 4.19\text{E}-02 \\ -3.56\text{E}-02 \\ 2.61\text{E}-02 \\ -7.22\text{E}-03 \\ 3.67\text{E}-03 \end{bmatrix}$	$\begin{bmatrix} 0.7953 \\ 5.8006 \\ -27.6754 \\ 11.2771 \\ 22.0526 \end{bmatrix}$

An energy compensation vector is then calculated for each SPM scintillator combination. These vectors are the weighting vectors applied to the corresponding channel intervals and are shown in figures (18-23).

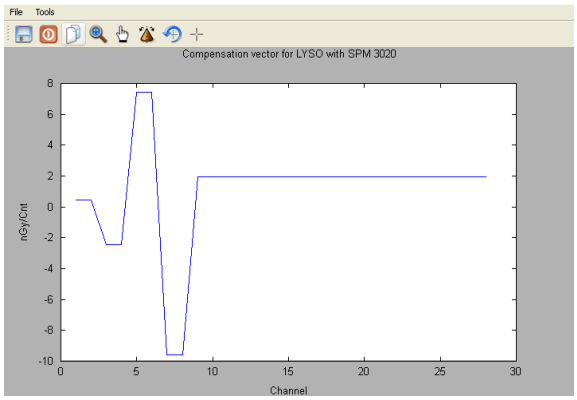

Figure 18 LYSO(Ce) with SPM 3020

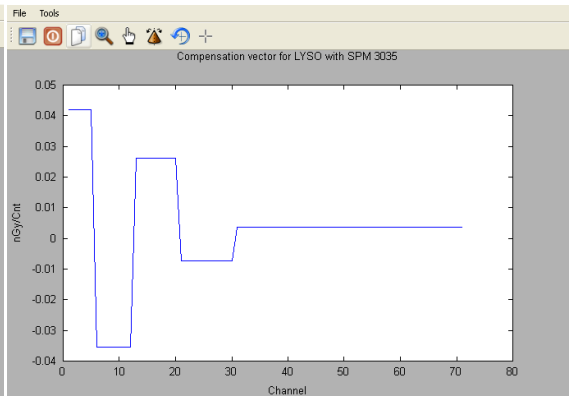

Figure 19 LYSO(Ce) with SPM 3035

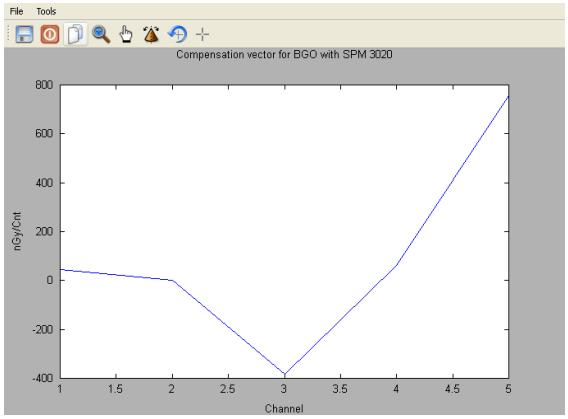

Figure 20 BGO with SPM 3020

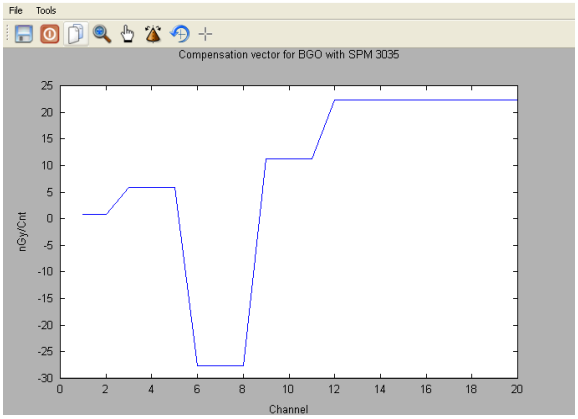

Figure 21 BGO with SPM 3035

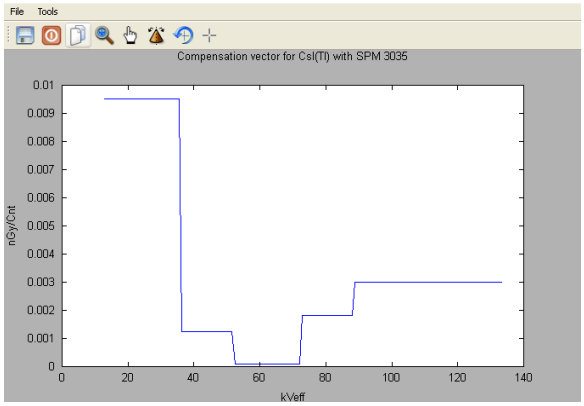

Figure 22 CsI(Tl) with SPM 3035

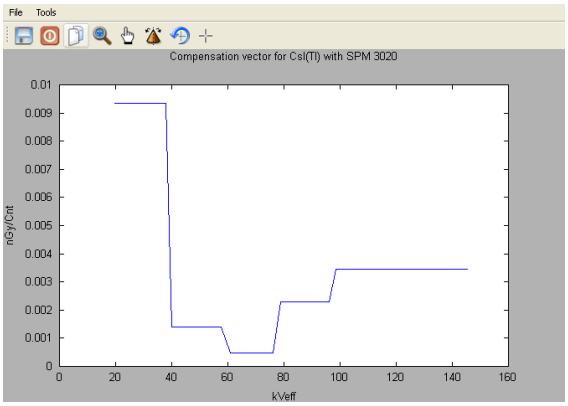

Figure 23 CsI(Tl) with SPM 3020

4.5 Stability

Before dosimetric calculations are made on dose rate test vectors a stability analysis of the energy compensation vectors are made. The stability depends on the balance between the factors in the weighting vectors. To investigate the stability of the energy compensation vectors errors are applied to each interval i.e. each factor in the weighting vector. The dose rates of the reference vectors are then calculated. Errors are applied to one interval at the time and the relative error compared to the reference vectors are calculated for each applied error. The results for the different vector sets with 1% applied error are displayed in table (2).

Table 2 Relative error in % for 1% applied error

	BGO	LYSO(Ce)	CsI(Tl)
SPM 3020	152.69	208.19	0.32
SPM 3035	64.20	1.60	0.33

The results in table (2) reflect the graphs over the energy compensation vectors in figures (18-23). For example LYSO with SPM 3020 flickers a lot and have two negative values resulting in very large relative error. Because of the high stability and well resolved spectrums for CsI(Tl) compared to the results for BGO and LYSO(Ce) the latter two are discarded for further analyze. The numbers of used channels are also parameters that affect the stability.

4.6 Dose rate calculations

For CsI(Tl) combined with both SPMs the dose rate for some different test vectors are calculated using the energy compensation vectors from above . The results for CsI(Tl) with SPM 3020 are presented in table (3). As discussed in chapter 4.1 the measuring equipment saturates at higher count rates which explain the poor performance on some of the vectors (marked red).

For lower count rates i.e. dose rates, the results are within a couple of percent. The reference dose rates are measured using the Unfors Xi survey probe.

Table 3 Test vectors for CsI(TI) with SPM 3020

Filter	mA	kV	Cnt/s	Reference dose rate (nGy/s)	Calculated dose rate (nGy/s)	Error (%)
N40	0.2	40	1033	8.44	8.15	-3.66
N60	0.2	60	1206	4.00	4.11	2.71
N60	0.2	70	3167	9.33	9.28	-0.62
N80	0.4	80	8019	19.11	19.05	-0.31
N80	0.4	90	4387	10.22	9.78	-4.56
N80	0.6	80	29998	117.78	75.81	-55.35
N100	0.6	100	13064	34.67	31.52	-9.98
N100	0.6	110	16879	52.44	43.58	-20.35
N120	0.6	120	5280	14.22	14.27	0.34
N120	0.8	120	17980	66.67	52.12	-27.92

In table (4) the reference vector that is used to calculate the compensation vectors for CsI(TI) with SPM 3020 is shown.

Table 4 Reference vectors for CsI(TI) with SPM 3020

Filter	mA	kV	ref dose (nGy/s)	Cnt/s
N40	0.3	40	57.33	7369
N60	0.3	60	26.67	7601
N80	0.4	80	20.00	8367
N100	0.5	100	11.56	5160
N120	0.6	120	14.67	5521

To illustrate the test vectors result and the saturation phenomena some of the test vectors are plotted in the reference spectrum in figures (24, 25).

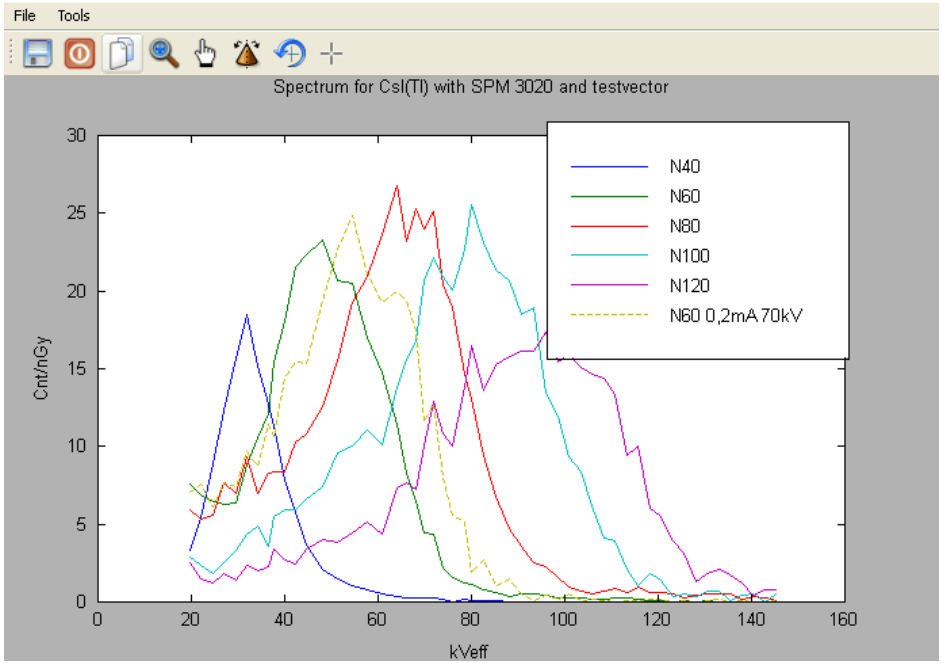

Figure 24 Test vector plotted in reference vector spectrum

In figure (24) the spectrum for N60 0.2mA 70kV are displayed, it can be seen that the peak is nicely placed between N60 and N80, the amplitude is also placed between the peaks of N60 and N80 which indicates that there is no saturation. The kVeff value according to the plot is 54.4 keV which corresponds well with the calculated value from SpekCalc of 53.3 keV.

In figure (25) N80 with different current is displayed, the saturation is clearly shown for the 0.6mA case since the amplitude is considerably lower and the “tail” does not have as sharp slope as the 0.4mA or the reference vector. These effects are due to pile up which makes the system detect fewer but higher peaks.

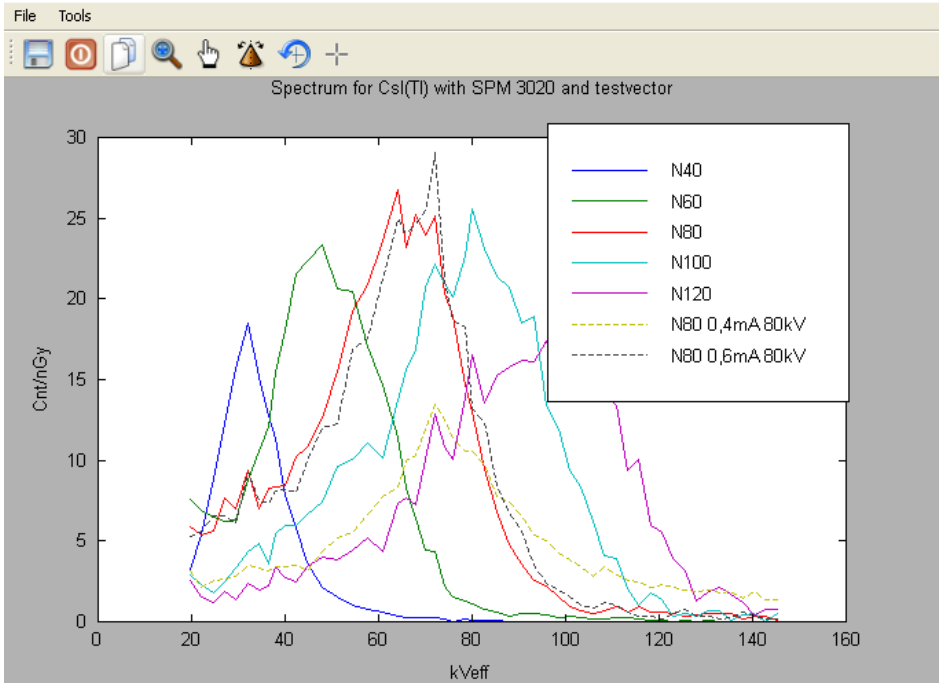

Figure 25 Test vectors plotted in reference vector spectrum

In table (5) the result for the test vectors for CsI(Tl) with SPM 3035 are shown.

Table 5 Test vectors for CsI(Tl) with SPM 3035

Filter	mA	kV	Cnt/s	Reference dose rate (nGy/s)	Calculated dose rate (nGy/s)	Error (%)
N40	0,2	50	1613	8.81	8.60	-2.43
N40	0.3	50	22170	133.22	97.47	-36.67
N60	0.3	70	5685	15.35	16.22	5.32
N80	0.4	90	7279	14.90	15.22	2.11
N100	0.5	110	4801	11.29	10.62	-6.33
N120	0.6	110	4873	11.74	11.48	-2.28

In table (6) the reference vector that is used to calculate the compensation vectors for CsI(Tl)with SPM 3035 is displayed.

Table 6 Reference vectors for CsI(Tl) with SPM 3035

filter	mA	kV	ref dose (nGy/s)	Cnt/s
N40	0.3	40	58.71	7997
N60	0.3	60	32.97	10103
N80	0.4	80	23.03	10511
N100	0.5	100	13.10	6141
N120	0.6	120	16.26	6472

Some of the dose rate test vectors for SPM 3035 are displayed in figures (26, 27).

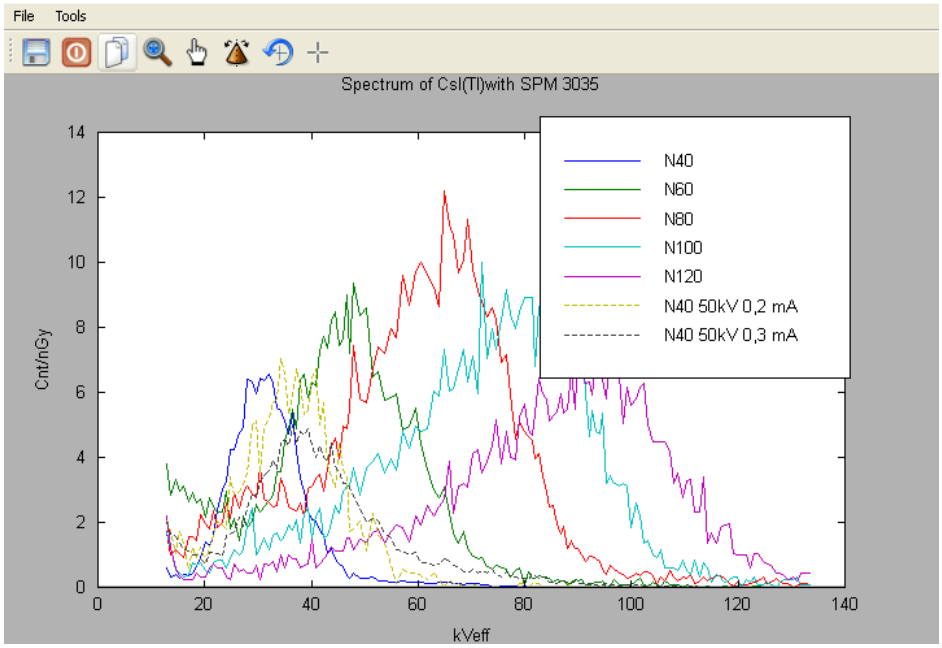

Figure 26 Test vectors plotted in reference vector spectrum

Figure (26) shows the two test vectors for N40 50 kV, the saturation in the 0.3 mA case is obvious and the 0.2 mA case shows a good result. Both correspond well to the results in table (5). The two dose rate test vectors for 110 kV are displayed in figure (27). The peaks are separated and have values from the graph of 79.1 and 94.7 keV compared to SpekCalc calculations of 90.1 and 95.1 keV. This is due to the higher amount of flicker that is the result of higher resolution in the SPM 3035. To get a more correct position of the peak an averaging of the spectrum could be used.

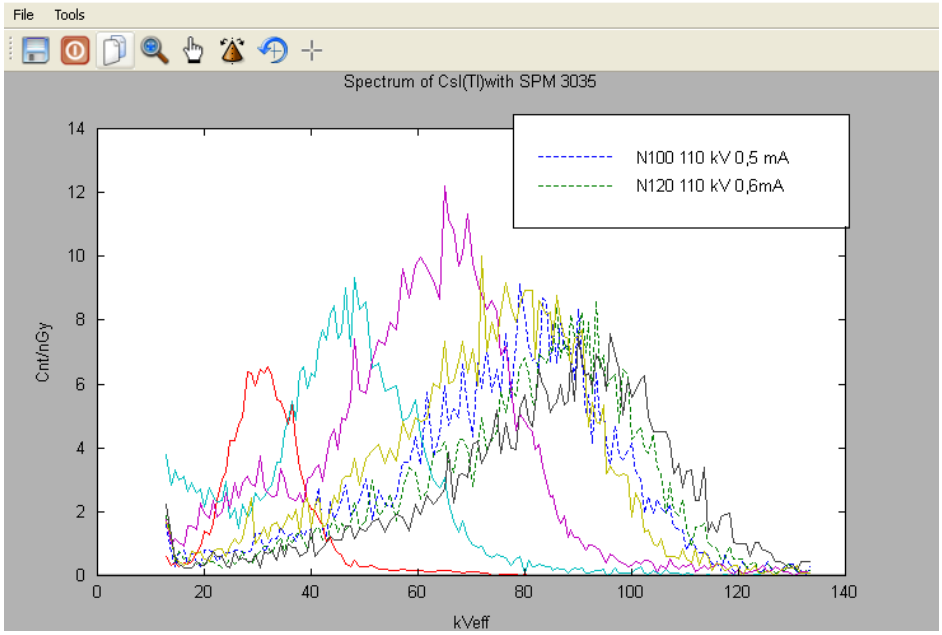

Figure 27 Test vectors plotted in reference vector spectrum

The relative errors for the dose rate test vectors with 1% applied error for SPM 3020 and SPM 3035 are displayed in table (7). The results yield a good stability towards noise.

Table 7 Relative errors with 1% applied error for all dose rate test vectors

SPM 3035	Filter	mA	kV	rel error (%)
	N40	0.2	50	0.40
	N40	0.3	50	0.38
	N60	0.3	70	0.36
	N80	0.4	90	0.28
	N100	0.5	110	0.25
	N120	0.6	110	0.27
SPM 3020	N40	0.2	40	0.43
	N60	0.2	60	0.35
	N60	0.2	70	0.33
	N80	0.4	80	0.28
	N80	0.4	90	0.23
	N80	0.6	80	0.25
	N100	0.6	100	0.23
	N100	0.6	110	0.25
	N120	0.6	120	0.27
	N120	0.8	120	0.29

4.5 Plastic scintillator

The plastic scintillator BC-428 was also evaluated. The lesser light yield made it difficult to detect low energies but the water equivalent composition states that every count regardless of energy can be related to a specific dose rate. The spectrum in figure (28) somewhat resembles BGO and the light yield are about the same.

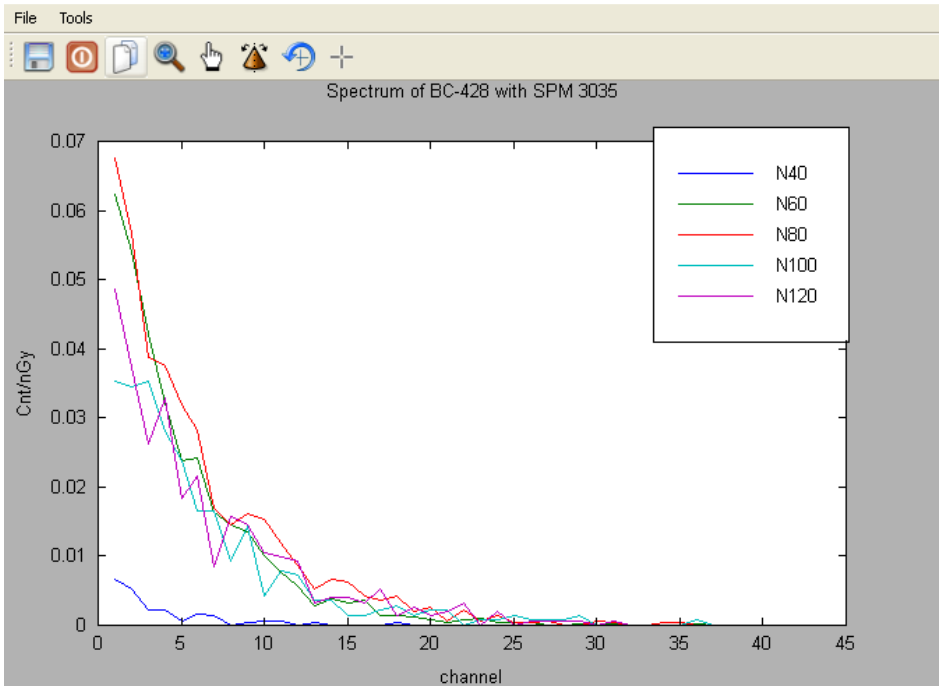

Figure 28 Spectrum for BC-428 with SPM 3035

The vectors plotted in figure (28) are displayed in table (8) and it can be seen on the graph that the sensitivity of BC-428 are very low compared to the others scintillators. This depends to the low density and atomic number which gives a low stopping power. With low atomic numbers the influence of the photoelectric effect is significantly decreasing and the energy deposit can be assumed to be dominated by Compton scattering. The Compton scattering is more concerned with impact angle than the energy of the incident X-ray photons which explains the uniform spectrum for N60-N120. For N40 the titanium dioxide in the reflective paint could be responsible for the weak signal.

Table 8 Vector values for BC-428

Filter	mA	kV	ref dose (nGy/s)	Cnt/s
N40	6	40	3043.59	68
N60	6	60	5703.69	1873
N80	6	80	3019.32	1168
N100	6	100	1388.30	362
N120	6	120	1524.22	440

4.6 Low energies (<32kV)

To investigate the ability to detect low energies, the L filtration series was used [Appendix A]. The N series could not be used since the dose rate was too high. I order to use the N series the distance to the X-ray tube has to be increased to reduce the dose rate. Reference dose rates were not possible to obtain since the ion chamber used for reference did not trigger at the used dose rates. However clear spectrum was collected with the CsI(TI) and SPM 3035. This means that there should not be any problems to apply the same method as in chapter 4.4 to do dosimetry at these energy levels.

The low energy spectrums in figure (29) are fitted on the kVeff x-axel from the N40-N120 spectrum taken with CsI(TI) and SPM 3035 to get a approximated kVeff value.

Figure (29) displays L20, L30 and L35 with a molybdenum anode and all the spectrums are well resolved. For L35 there is saturation in the measuring setup due to high dose rate but the peak is still well resolved. The spectrum for N30 filtration with 20 kV are also displayed in figure (29) and has a kVeff value from SpekCalc of 18keV which corresponds excellent with the value from the graph which is also 18 keV. The theoretical value for L20 is not possible to obtain using SpelCalc or Spectrum Processor and that is why the N30 20 keV spectrum is displayed. For L30 the Spectrum Processor yields a kVeff of 26.5 keV for the molybdenum anode which is the same as for the wolfram anode. Because of that the kVeff value for L20 and L35 with a molybdenum anode are assumed to be the same as for a wolfram anode. Hence it can be stated that the L20 spectrum has a kVeff of ~17 keV and that the measuring setup can handle energies of at least that.

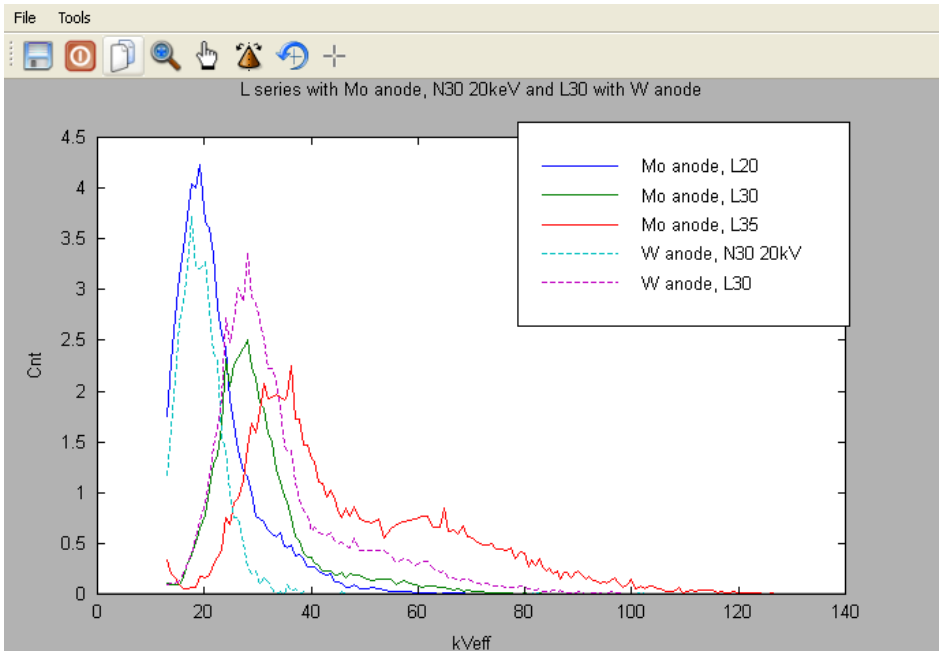

Figure 29 Low energies spectrum

4.7 Background measurement

To demonstrate the sensitivity of the system a measurement of the background radiation was performed. Spectrums were taken with and without a “lead cave”, the fact that there is a significant difference between the two spectrums indicates that the signal is background and not noise. CsI(Tl) was used together with SPM 3035. Data were collected during 10 min and the background radiation were estimated to one CPS. The reference dose rate where measured using an ion camber. The size of the CsI(Tl) scintillator was 15x3x3 mm.

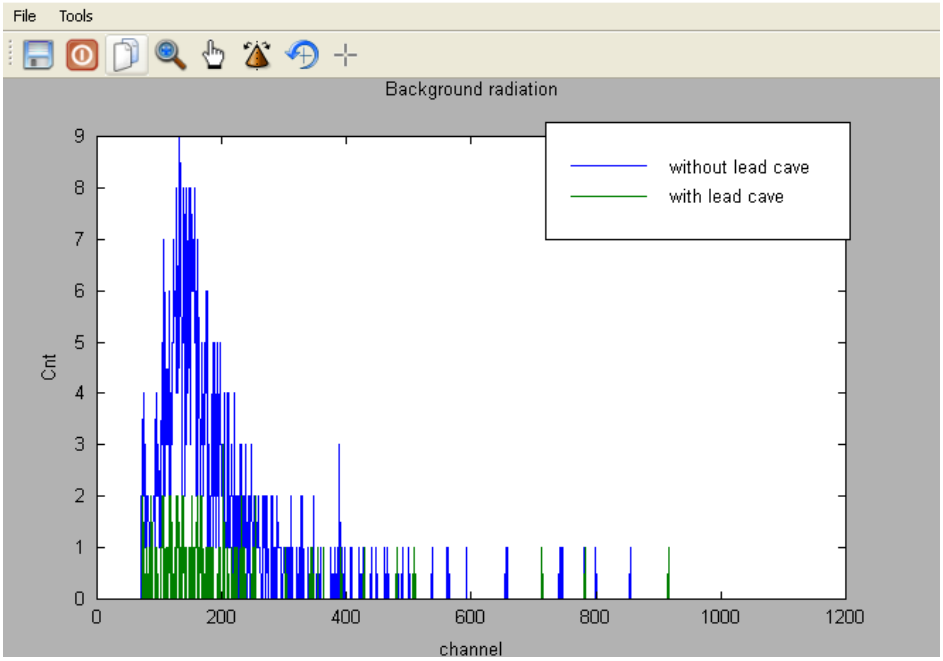

Figure 30 Histogram of background radiation with CsI(TI) and SPM 3035

The total amount of counts with and without the lead cave is displayed in figure (30) and in table (8). The initial peak is due to the aluminum box that shields the detector from the lowest energies.

Table 8 Background measurements with CsI(TI) and SPM 3035

	Cnt/10min	reference dose rate (nGy/10min)	Cnt/nGy
without lead cave	700	16,67	42
with lead cave	100	2,38	42

4.8 Temperature dependence

The SPM are able to operate well in room temperature but the characteristics are not unchanged with temperature. The noise and the gain are the parameter that is mainly affected. If dosimetry is performed with the method mentioned above the increase in gain will disturb the dose rate calculation since the spectrum is shifted to the right, an example of this is

shown in figure (31). To do correct dosimetry at varying temperatures this problem has to be compensated for. A possible solution could be to vary the overbias with temperature since the relationship between overbias and gain is linear.

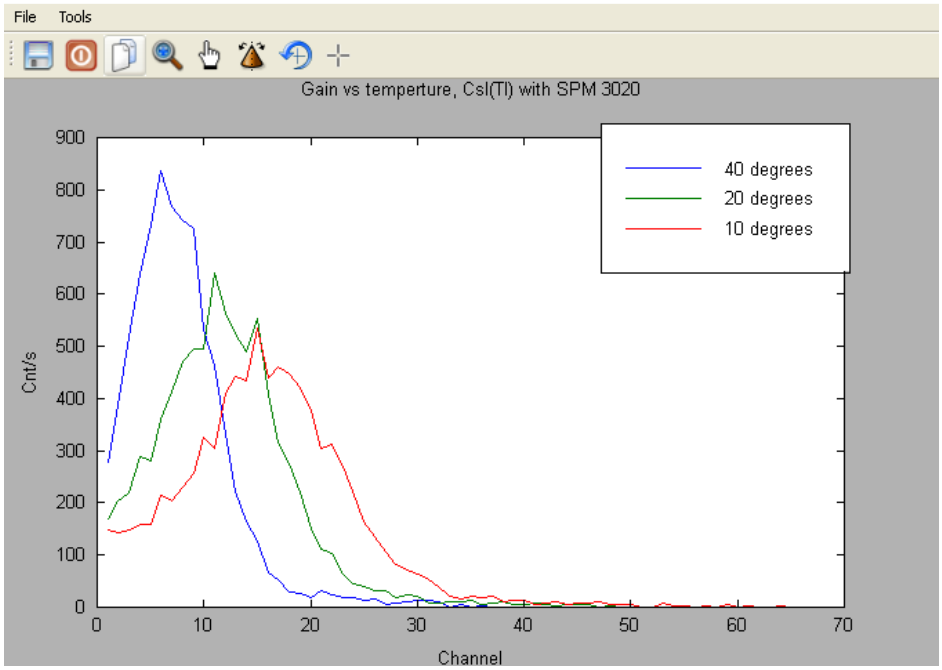

Figure 31 Gain for N80 80kV 0,4 mA at different temperatures

The difference between 10 degrees and 40 degrees is 9 channels. For CsI(Tl) with SPM 3020 one channel is >2kV resulting in an possible error of the detected signal with about 20kV.

The frequency of the noise depends strongly on the temperature but since all measuring are made at a threshold above the noise this is not as big a problem as the increase in gain. If however even lower energies are of interest and the measuring has to take place within the noise the reduced noise levels at lower temperatures are of great relevance. The temperature dependence of the noise is shown in figures (32, 33). At higher temperature the noise level are almost identical at 30 degrees but at 44 the noise level increases markedly. The initial drop in counts for the 44 degree curve is due to saturation in the measuring circuitry.

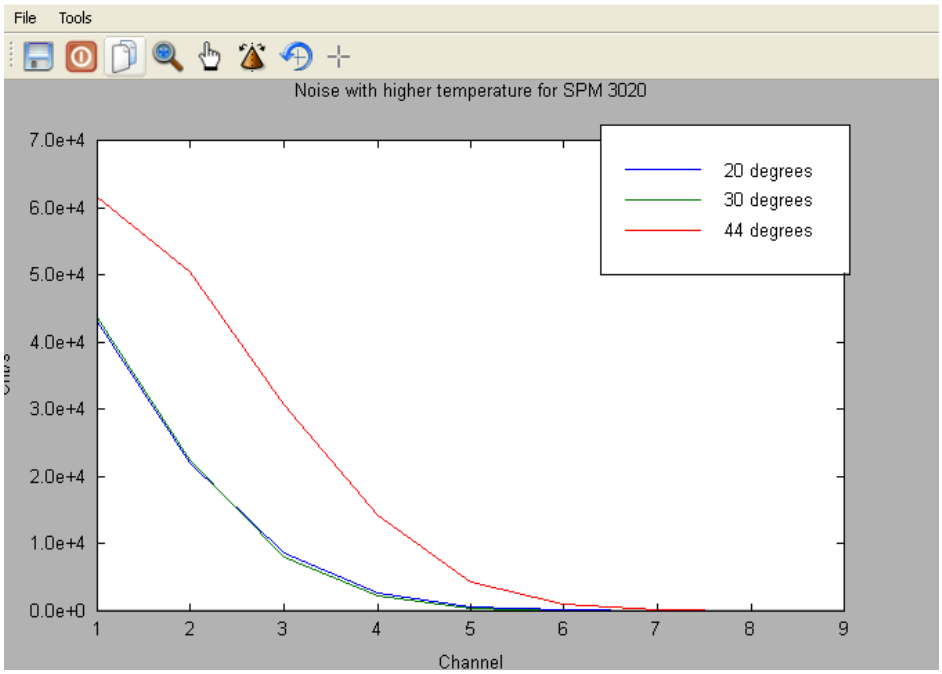

Figure 32 Noise with higher temperature

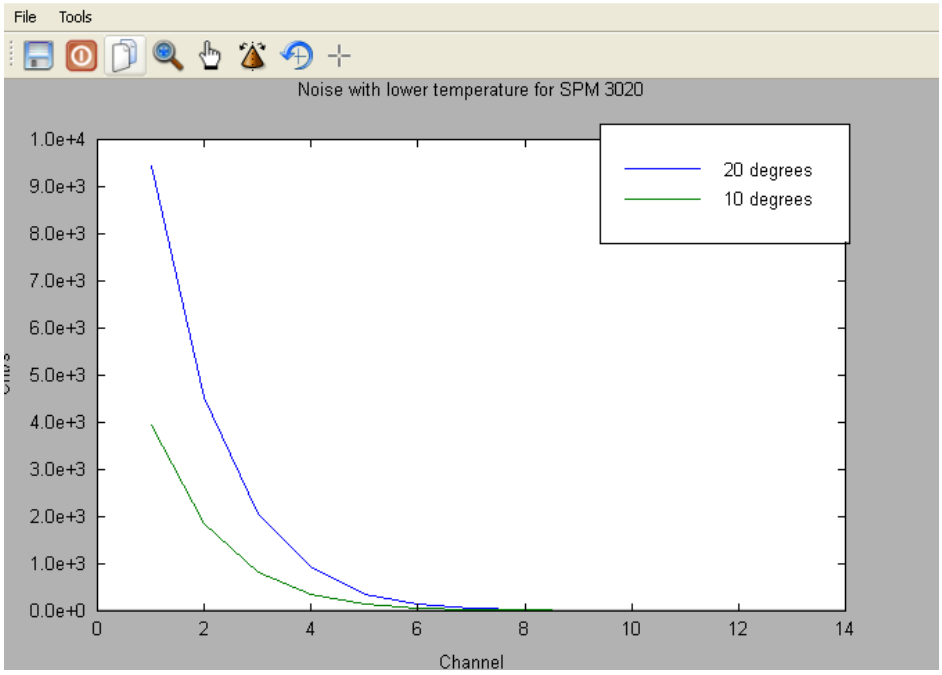

Figure 33 Noise with lower temperature

5 Conclusion & Discussion

Table 9 keV_{low} for different combinations

	CsI(Tl)	LYSO(Ce)	BGO	BC-428
SPM 3020	32 keV	>96keV	>96keV	>96keV
SPM 3035	17 keV	64keV	>96keV	>96keV

Table (9) shows at what energies the different detector combinations resolve more than ~90% of the signal, CsI(Tl) are by far the best scintillator at low energies. This is due to the high light yield and reasonably high stopping power.

LYSO(Ce) has benefits when high counting rates are important because of its short decay time (40ns) but the light yield is not enough to resolve energies below 64keV.

BGO could be useful at higher energies, because of the high density and high atomic number the photoelectric effects will have a greater influence at higher energies than for the other scintilators.

These conclusions are made with the noise levels in the experimental setup, with lower noise the energy range for usefulness will go down for all combinations.

Dosimetry with a SPM 3035 and CsI(Tl) is proven to work between 17-96keV

BGO, LYSO(Ce) and BC-428 are discarded for dosimetric evaluation in this energy range because they have to low light yield to resolve a spectrum. This may be dealt with by using a SPM with higher PDE or reducing the noise level, but since the spectrum from BGO and BC-428 are so poorly resolved they are still not likely to be useful. LYSO(Ce) combined with SPM 3035 would however not need as much increase in performance to be able to operate in the used energy range.

Possible improvement of the setup could be to use an active quenching technique in the SPM to achieve lesser reset time of the Geiger mode silicon photodiodes and hence get a higher

bandwidth. This would enable higher counting rates but the SPM electronics would be more complex. For this to be useful the decay time of the scintillator has to be less than about 100 ns that is the current quenching time.

For the SPMs the smaller PDE and the higher amount of microcells of the SPM 3020 allows for higher photon fluxes but this is not necessary for this energy range. The trade off to large dynamic range is worse photon detection efficiency resulting in a lower “gain” of the incident radiation, hence more difficult to resolve the signal from the noise. For optimal performance on a given energy range the SPM should have the right amount of microcells i.e. the right size of the microcells for a given area. This needs to be optimized against a specific scintillator due to the large differences in the characteristics for different scintillator materials. With a variable overbias the dynamic range could be changed depending on the energies of interest, perhaps with a high low switch on a possible instrument.

Since the SPM has a theoretical maximum bandwidth of 10 MHz due to the quenching circuit a potential dosimeter with higher sampling rate would be able to handle higher dose rates than the ones used in this thesis before the saturation becomes a problem. To manage even higher dose rates some filtration could be used to reduce the dose rate. There is also the possibility to used more than one channel to get a better PDE on a wider energy spectrum.

6 Future work

Investigate the upper energy limit before saturation for the different detection solutions.

Optimize the dynamic range for intended energy range by adjusting the overbias and thereby changing the PDE, or increase the fill factor i.e. increase the microcell size on a fixed area.

Test the detection solutions with a higher sampling rate to investigate the upper dose rate limit.

With a small dynamic range how low energies can be detected, for example with SPM 3050.

References

[1] Knoll G.F ,(2000), *Radiation Detection and Measurement,* New York: John Wiley & Sons, Inc.

[2] *SPM Scintillator Pack User Guide,* Sensl, 2007

[3] Y.Koba et al.,"*Light Output Response of LYSO(Ce) Crystal to Relativistic Helium and Carbon Ions", IEEE Nucl. Sci. Symposium Conference Record,* Vol.3, pp 2303-2306, 2007

[4] J.B Birks, (1964), *The Theory and Practice of Scintillation Counting,* Oxford: Pergamon Press

[5]"*MPPC, Multi-Pixel Photon Counter",* (Electronic Reference). Available: <http://sales.hamamatsu.com/assets/pdf/catsandguides/mppc_kapd0002e07.pdf>. (2010-12-14).

[6]*" APD Arrays: Geiger-mode APD arrays detect low light"* (Electronic Reference). Available: <http://www.optoiq.com/index/photonics-technologies-applications/lfw-display/lfw-article-display/335986/articles/laser-focus-world/volume-44/issue-8/features/apd-arrays-geiger-mode-apd-arrays-detect-low-light.html>. (2010-12-14).

[7] "*Geiger-Mode Avalanche Photodiodes for Three-Dimensional Imaging"* , (Electronic Reference). Available: <http://www.ll.mit.edu/publications/journal/pdf/vol13_no2/13_2geigermode3d.pdf>. (2010-12-14).

[8] "*Reversed biased P-N junction*", (Electronic Reference). Available: <http://hyperphysics.phy-astr.gsu.edu/hbase/solids/diod.html#c2> . (2010-12-15).

[9] R.Mita et al.,"*A fast active quenching and recharging circuit for single-photon avalanche diodes"*, *Proceedings of the European Conference on Circuit Theory and Design,* Vol.3,pp 385-388, 2005

[10] "*BC-428 Green-Emitting Plastic Scintillator*" (Electronic Reference). Available: <http://www.detectors.saint-gobain.com/uploadedFiles/SGdetectors/Documents/Product_Data_Sheets/BC428-Data-Sheet.pdf>. (2010-12-14).

[11] A.-M.Frelin et al., "*Comparative Study of Plastic Scintillators for Dosimetric Applications" IEEE Trans . Nucl. Sci.*,pt.2, vol.55, pp 2749-2756, 2008

[12] "*Photomultiplier tubes, basics and applications, third edition",.* (Electronic Reference). Available: <http://sales.hamamatsu.com/assets/applications/ETD/pmt_handbook_complete.pdf>. (2010-12-08).

[13] "*ScintPack1, SPM Scintillator Demonstrator Pack*", (Electronic Reference). Available: <http://sensl.com/downloads/scintpack1_datasheet.pdf >. (2010-12-14).

[14] "*SPMMicro Low Cost High Gain APD*", (Electronic Reference). Available: < http://sensl.com/downloads/spmmicro_datasheet1.pdf >. (2010-12-14).

[15] M.Marisaldi et al*.,"X- and gamma-ray detection with a silicon drift detector coupled to a CsI(TI) scintillator operated with pulse shape discrimination technique" IEEE Trans . Nucl. Sci.*, pt.3, vol. 52, pp 1842-1848, 2005

[16]"*MPPC, Multi-Pixel Photon Counter",* (Electronic Reference). Available: <http://sales.hamamatsu.com/assets/applications/SSD/mppc_kapd9003e02.pdf>. (2010-12-14).

[17]A.G. Stewart et al., "*Performance of 1-mm^2 Silicon Photomultiplier" , IEEE Journal of Quantum Electronic*s, vol.44, no2, pp 157 – 164, Feb. 2008

[18]J.L. Prince, J.M Links, (2005), *Medical Imaging Signals and System,* New Jersey: Prentice Hall

[19]S.Espana et al., "*Performance Evaluation of SiPM Detectors for PET Imaging in the Presence of Magnetic Fields", IEEE Nucl. Sci. Symposium Conference Record,* pp 3591-3595, 2008

[20] M. Mazzillo et al., "*Quantum Detection Efficiency in Geiger Mode Avalanche Photodiodes", IEEE Trans . Nucl. Sci,* pt.2, vol.55, pp 3620-3625, 2008

[21] *"Polyvinyltoluene, mixed isomers"* (Electronic Reference). Available: < http://www.chemindustry.com/chemicals/056814088.html>. (2010-12-08).

[22]S.Vasile, J. Rau,"*Geiger sensor arrays for microvertex applications " IEEE Nucl. Sci. Symposium Conference Record,* vol.3, pp 1633-1635, 2006

Appendix A

Table 3 — Characteristics of low air-kerma rate series

Mean energy, $\overline{E}$ keV	Resolution, R_E %	Tube potential[1] kV	Additional filtration[2] mm				1st HVL[4] mm
			Pb	Sn	Cu	Al	
8,5		10				0,3[3]	0,058 Al
17	21	20				2,0[3]	0,42 Al
26	21	30			0,18	4,0[3]	1,46 Al
30	21	35			0,25		2,20 Al
48	22	55			1,2		0,25 Cu
60	22	70			2,5		0,49 Cu
87	22	100		2,0	0,5		1,24 Cu
109	21	125		4,0	1,0		2,04 Cu
149	18	170	1,5	3,0	1,0		3,47 Cu
185	18	210	3,5	2,0	0,5		4,54 Cu
211	18	240	5,5	2,0	0,5		5,26 Cu

1) The tube potential is measured under load.

2) Except for the three lowest energies, where the recommended inherent filtration is 1 mm of beryllium, the total filtration consists of the additional filtration plus the inherent filtration, adjusted to 4 mm of aluminium (see 4.2.3).

3) The recommended inherent filtration is 1 mm Be, but other values may be used provided tht the mean energy is within ± 5 % and the resolution is within ± 15 % of the values given in the table.

4) The HVLs are measured at 1 m from the focal spot. The second HVL is not included for this series, since it is not significantly different from the first HVL.

Table 4 — Characteristics of narrow-spectrum series

Mean energy, $\overline{E}$ keV	Resolution, R_E %	Tube potential[1] kV	Additional filtration[2] mm				1st HVL[4] mm	2nd HVL[4] mm
			Pb	Sn	Cu	Al		
8	28	10				0,1[3]	0,047 Al	0,052 Al
12	33	15				0,5[3]	0,14 Al	0,16 Al
16	34	20				1,0[3]	0,32 Al	0,37 Al
20	33	25				2,0[3]	0,66 Al	0,73 Al
24	32	30				4,0[3]	1,15 Al	1,30 Al
33	30	40			0,21		0,084 Cu	0,091 Cu
48	36	60			0,6		0,24 Cu	0,26 Cu
65	32	80			2,0		0,58 Cu	0,62 Cu
83	28	100			5,0		1,11 Cu	1,17 Cu
100	27	120		1,0	5,0		1,71 Cu	1,77 Cu
118	37	150		2,5			2,36 Cu	2,47 Cu
164	30	200	1,0	3,0	2,0		3,99 Cu	4,05 Cu
208	28	250	3,0	2,0			5,19 Cu	5,23 Cu
250	27	300	5,0	3,0			6,12 Cu	6,15 Cu

1) The tube potential is measured under load.

2) Except for the five lowest energies, where recommended inherent filtration is 1 mm Be, the total filtration consists of the additional filtration plus the inherent filtration, adjusted to 4 mm of aluminium (see 4.2.3).

3) The recommended inherent filtration is 1 mm Be, but other values may be used provided that the mean energy is within ± 5 % and the resolution is within ± 15 % of the values given in the table.

4) The HVLs are measured at 1 m from the focal spot.